# Insights into machining techniques for additively manufactured Ti6Al4V alloy: a comprehensive review.

SAMBO, A.M., YOUNAS, M. and NJUGUNA, J.

2024

*applied sciences*

MDPI

*Review*

# Insights into Machining Techniques for Additively Manufactured Ti6Al4V Alloy: A Comprehensive Review

**Abdulkadir Mohammed Sambo, Muhammad Younas * and James Njuguna**

School of Computing, Engineering and Technology, Robert Gordon University, Aberdeen AB10 7GJ, UK; a.sambo1@rgu.ac.uk (A.M.S.); j.njuguna@rgu.ac.uk (J.N.)
* Correspondence: m.younas@rgu.ac.uk

**Abstract:** Investigation into the post-processing machinability of Ti6Al4V alloy is increasingly crucial in the manufacturing industry, particularly in the machining of additively manufactured (AM) Ti6Al4V alloy to ensure effective machining parameters. This review article summarizes various AM techniques and machining processes for Ti6Al4V alloy. It focuses on powder-based fusion AM techniques such as electron beam melting (EBM), selected laser melting (SLM), and direct metal deposition (DMD). The review addresses key aspects of machining Ti6Al4V alloy, including machining parameters, residual stress effects, hardness, microstructural changes, and surface defects introduced during the additive manufacturing (AM) process. Additionally, it covers the qualification process for machined components and the optimization of cutting parameters. It also examines the application of finite element analysis (FEA) in post-processing methods for Ti6Al4V alloy. The review reveals a scarcity of articles addressing the significance of post-processing methods and the qualification process for machined parts of Ti6Al4V alloy fabricated using such AM techniques. Consequently, this article focuses on the AM-based techniques for Ti6Al4V alloy parts to evaluate and understand the performance of the Johnson–Cook (J–C) model in predicting flow stress and cutting forces during machining of the alloy.

**Keywords:** additive manufacturing; direct metal deposition; tool wear; energy consumption; optimization; qualification; machining operation; Johnson–Cook model; Ti6Al4V alloy



**Citation:** Sambo, A.M.; Younas, M.; Njuguna, J. Insights into Machining Techniques for Additively Manufactured Ti6Al4V Alloy: A Comprehensive Review. *Appl. Sci.* **2024**, *14*, 10340. https://doi.org/10.3390/app142210340

Academic Editor: Amit Bandyopadhyay

Received: 18 September 2024
Revised: 1 November 2024
Accepted: 5 November 2024
Published: 11 November 2024



## 1. Introduction

This paper presents a systematic review of the literature on the machinability of additively manufactured Ti6Al4V alloy, focusing on energy consumption, the qualification process of machined parts for assembly, and the effects of the tool wear rate. The review specifically addresses AM-based techniques for producing Ti6Al4V components and examines post-processing methods to evaluate machining performance responses, including tool wear rate, surface quality, chip morphology, and the optimization of cutting parameters. Additionally, it explores the application of the Johnson–Cook (J–C) model as a finite element analysis (FEA) tool to predict flow stress, cutting forces, and temperature fields during turning operations to achieve the desired final surface quality. The article begins by analyzing the properties, applications, advantages, and disadvantages of Ti6Al4V alloy as the material of focus.

The AM techniques reviewed include selective laser melting, laser metal deposition, electron beam melting, gas tungsten arc welding, the plasma arc welding process, and direct metal deposition. The machinability of the titanium alloy covered includes cutting tool material, tool geometry, tool wear rate, chip morphology, specific cutting energy, surface roughness, cutting forces, optimization processes, and qualification of machined parts for assembly.

AM is a promising technology that is capable of manufacturing metallic parts in a layer-by-layer manner. AM has vast advantages of reducing lead time, cost, and energy

consumption both in process energy consumption and wholistically due to material saving, stocking decrease, and assembly line reduction. The motivation behind AM is the need to automate machines to minimize waste material, reduce energy consumption, and improve material efficiency [1]. Moreover, the overall decline in component weights, especially in aerospace and automotive structural parts, significantly reduces energy consumption during their service period.

The lack of surface finishing is the only challenge of metal AM processed factors, which leads to post-processing (end-machining) requirements, especially at mating surfaces in an assembly. Manufacturing is energy-intensive, and techniques are developed to reduce energy consumption, especially in machining. Manufacturing accounts for 60% of the total energy used in the industry [2–4]. However, the cited references did not account for the energy consumption specifically associated with the machining process for titanium alloy. This review will help in understanding the amount of energy consumed by the machining process. Despite its advantages, the post-processing of AM parts still consumes power and needs to be investigated and optimized. The energy used in machining processes typically comes from various sources, such as electricity and fossil fuels, which can often be carbon-intensive. Reducing energy consumption decreases the demand for these energy sources, thus leading to lower carbon emissions.

The machining process involves the removal of unwanted material from a workpiece to achieve the desired surface finish. It is a critical and versatile method utilized across various industries, including the aerospace, automotive, and electronics fields. Machining processes are essential for the production of precise and complex components, ranging from simple parts to intricate prototypes.

Machining plays a central role in the manufacturing of a wide array of products, from everyday items like screws and bolts to critical components in industries like aerospace and medical devices. It is a versatile and indispensable manufacturing process that continues to evolve with advances in technology and materials, enabling the creation of increasingly complex and precise parts [5]. Apart from the poor surface finishing and low dimensional accuracy of AM titanium alloy, the mechanical and geometrical requirements of the aerospace industry are the main reasons for adopting the end-machining process as the most common approach to finish AM parts [6]. Figure 1 represents the ultimate tensile strength of classes of Ti alloys compared to the ASTM standard.

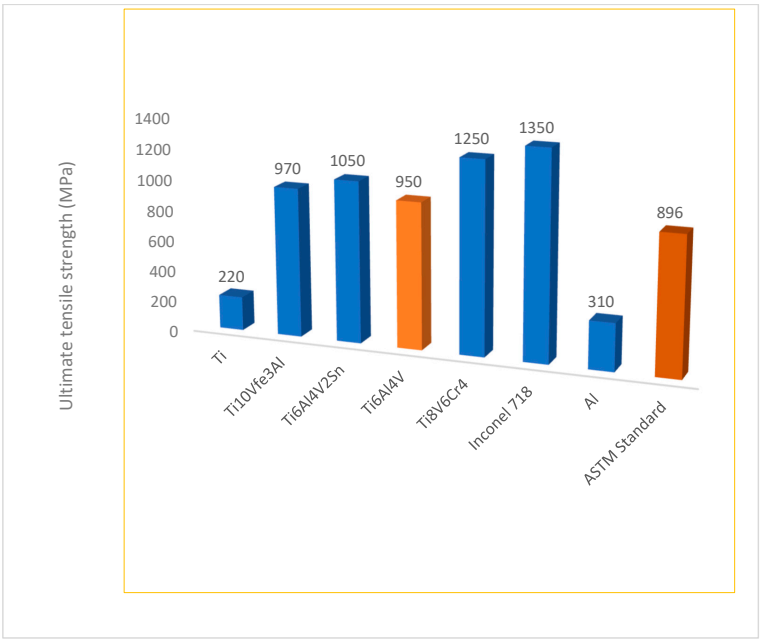


**Figure 1.** Ultimate tensile strength of Ti6Al4V alloy compared with other materials [7].

*Motivation of the Study*

This review paper aims to provide a comprehensive understanding of the state-of-the-art in the machining of additively manufactured Ti6Al4V parts. The areas to be addressed include the following.

- Significance of Ti6Al4V alloy
- Advancement and integration of additive manufacturing with conventional/traditional machining will help to bridge the gap between the two manufacturing processes and enhance process efficiency.
- A review of cutting parameters, including cutting speed, feed rate, and depth of cut, is crucial for improving surface roughness and tool life. By considering existing studies, this analysis can inform future research and enhance industrial practices. Optimizing these parameters can reduce cutting energy, contributing to sustainable manufacturing and supporting economic viability.
- Technical challenges such as tool wear and tool life: Ti6Al4V alloy is known as a difficult-to-cut material, posing significant tool wear. A review of existing studies will help to determine a durable material for cutting AM Ti6Al4V parts.
- Research gaps: A review of existing studies will highlight areas where current research is lacking and suggest the direction for future studies.

## 2. Additive Manufacturing Techniques

Metallic AM techniques can be broadly classified according to feedstock type, powder-fed or powder-bed fusion processes, and heat source type (laser or electric). Laser AM employs a gas or solid-state optical device with a focusing lens that produces a laser energy beam through rays. The advantages of a laser heat source include a small heat-affected zone, but high reflectivity is a drawback [8]. AM processes such as selective laser melting (SLM), direct metal deposition (DMD), and wire-based fusion employ laser heat energy to melt the feedstocks. Feedstock in additive manufacturing can be either wire-based or powder-based. Examples include wire arc additive manufacturing (WAAM) for wire-based processes and selective laser melting (SLM) for powder-based processes.

- Powder-bed fusion is an additive manufacturing process in which a layer of metallic powder is deposited and selectively melted using a laser or electron beam. Common techniques within this category include direct metal laser sintering (DMLS), electron beam melting (EBM), and selective laser melting (SLM).

Powder-fed fusion is an additive manufacturing process in which both the feedstock and laser energy are delivered through the same source. Common examples of this technique include direct metal deposition (DMD), laser additive deposition (LAD), and thermal spraying. Figure 2 shows a comparison of machining using different additive manufacturing techniques, obtained from a systematic literature review. However, the cited reference does not specify the criteria used for article selection, which represents a limitation of the paper. Different metallic AM techniques are described in Figure 3.

Laser-based AM processes are subject to a significant degree of induced residual stresses [9,10], which in Ti6Al4V AM are typically $5 \times 10^4$ K/cm [11]. The maximum stress value always occurs at or just below the surface, and the ultimate residual stresses will rise as the number of layers increases. According to the free surface of the final deposited layer, the residual stress profile is composed chiefly of tensile stresses at the top section of the material, the value of which is equivalent to the yield strength of a component [12]; adding a new layer causes compressive stress in the layers below the previous one to increase and tensile stress in the top layers to change into compressive stress [13,14]. Also, as the scan length advances, so do residual strains [10] representing various stresses of a different material at some selected tool geometry, cutting speed, and nose radius.

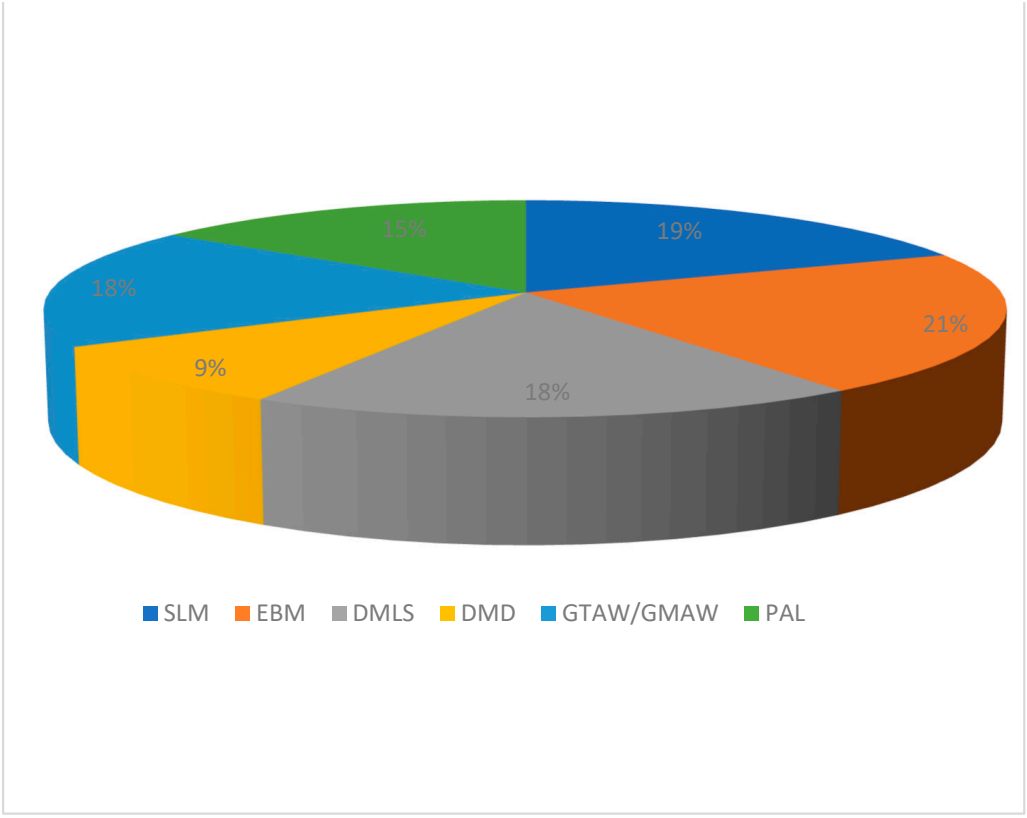


**Figure 2.** Comparison of machining processes for parts manufactured with different additive manufacturing techniques [7].

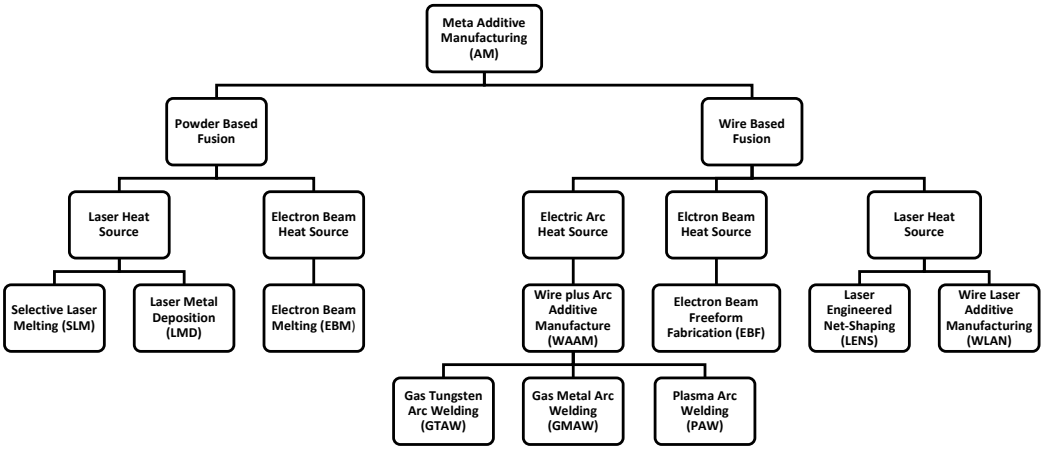


**Figure 3.** Classification of additive manufacturing processes [1].

### *2.1. Selective Laser Melting*

SLM is a powder-based AM process that utilizes laser energy to melt powder particles for the production of intricate components. This process is primarily suited for low-melting-point materials, such as aluminum and titanium. Reports indicate that the turning operations for Ti6Al4V alloy produced via the SLM process are associated with high cutting forces and increased surface roughness [15]. High feed rates and cutting speeds result in poor surface finishes in the turning of Ti6Al4V alloy parts produced from the SLM process compared to conventionally manufactured Ti6Al4V alloy parts; this is because the SLM process uses materials with high hardness and higher strength properties, which affect the plasticity of the materials. SLM process produces parts with relatively high residual

stresses; this is because of high mechanical and thermal loading during the manufacturing process [16].

In the milling operation for Ti6Al4V alloy parts made from the SLM process, it was observed that flow stress decreases at high temperatures and strain rates. Also, the cutting forces decrease when the cutting speeds reach 80 m/min [17]. Many researchers have reported on the machinability of Ti6Al4V alloy parts manufactured by the SLM process [18–21]. Many of the cited papers exhibit a common limitation by focusing exclusively on the selective laser melting (SLM) technique for manufacturing Ti6Al4V alloy parts and employing specific scanning strategies. Consequently, the findings may not be generalizable to other alloys or additive manufacturing (AM) techniques without proper validation. The Ti6Al4V melt pool produced by SLM has an optimal temperature of around 2710 K and cools at a rate of roughly $10^4$–$10^6$ K/s [12]. Another report employed multiple lasers to replace the traditional laser powder bed fusion process. The results show that the energy absorption rate increased by 14%, with a recorded cooling rate of 600 °C/s [22].

### 2.2. Direct Metal Laser Sintering

DMLS is a powder-based AM technique that employs laser energy to melt powder particles. This process can be used to melt metal with a high melting point, unlike SLM, such as cobalt, steel, and chromium, in addition to aluminum and titanium. Feed rates were reported to affect cutting forces and temperature fields at a higher speed than the cutting speed in the milling operation for Ti6Al4V alloy parts manufactured from the DMLS process. Continuous chip formation was also observed [23]. Chip adhesion and microchipping were also responsible for the tool wear [23]. However, higher residual stresses were generated compared to dry cutting in the turning operation for Ti6Al4V alloy parts manufactured from the DMLS process [24]. Continuous chip formation was observed in the drilling operation for Ti6Al4V alloy parts fabricated from the DMLS process, and microchipping and chip adhesion were observed [25]. Many studies reported the machinability of Ti6Al4V alloy parts fabricated from the DMLS process [26–28].

### 2.3. Electron Beam Melting

EBM is the primary heat source for AM technology, melting metals by using the cathode of a beam gun through the anode, which might be a charged filament. This has the advantage of high power density, hence high heat imparts melting, and in turn reduces defects and residual stress [8]. DMLS/SLM: Surface defects that arise include surface roughness and porosity due to incomplete melting of powder particles; spatter is caused by the laser. These can be minimized through the optimization of process parameters or the application of post-processing techniques like machining or polishing. Electron Beam Melting: EBM has lower defects because of the high amount of heat applied during melting; hence, the defects and residual stresses are significantly low as compared to other AM techniques, such as powder bed fusion processes like SLM. In comparison to conventionally produced parts, the microhardness of Ti6Al4V alloy parts produced from EBM and DMLS has been observed to have 21% and 26% higher microhardness, respectively [27]. Results indicated that EBM exhibits a cooling rate of around $10^6$ K/min and an equivalent cooling rate of about $7 \times 10^4$ K/s during the AM fabrication process for Ti6Al4V alloy parts [12,29].

### 2.4. Direct Metal Deposition

DMD is a powder-fed fusion process capable of additively manufacturing large-scale complex metallic parts, unlike SLM, DMLS, and EBM. This process has the advantage of creating a layer thickness of up to 2 mm. The laser scanning speed is the most critical factor in determining whether the final parts manufactured have acceptable dimensions and properties.

The compressive stresses were observed to be the common factor in DMD wire-based manufacturing of Ti6Al4V alloy parts [30]. Therefore, the cutting forces are greatly affected by the nature of the stresses developed during the manufacturing process. A 300 °C preheating temperature was applied to reduce the effect of temperature build-up during side milling of DMD-manufactured Ti6Al4V alloy parts; the results showed a significant reduction in the milling forces observed, which was due to the thermal softening effect in the titanium part [31]. Preheating the workpiece before the machining operation could increase the tool's life. This research focuses exclusively on the Ti6Al4V alloy, omitting the exploration of other alloys. It investigates milling forces and temperature effects only at 300 °C and above, neglecting lower temperatures and extreme conditions. Additionally, the study does not consider other machining responses, such as tool wear rate, residual stresses, or microstructural changes.

There needs to be more reported literature on the DMD powder-based fusion process. Selection of the best laser scanning process parameters results in minimal or zero defects in the specimen. Reports show 850, 1000, 1250, and 1500 mm/s were selected for laser scanning speed; 55% to 100% for laser power, depending on the machine's maximum power output ($P_{max}$ = 200 W); spot size: smaller (S), medium (M), and large (L)—based on the settings specific to the machine (from 150 µm to 250 µm); the layer always had a 40 µm thickness [29]. The larger spot size was prepared, and a 1250 mm/s scanning speed resulted in less porosity within the temperature fields [29]. The melt pool region's optimum temperature is an independent singularity higher than the temperature at which Ti-6Al-4 V vaporizes. The design of a laser scanning technique should incorporate a considerable scan beam length that uniformly rotates the scan vector directions, thereby creating an isotropic stress distribution within the part. In each case, the hatched area is scanned first, followed by a single outer contour. The surface temperature of a single scan vector approximates a melt pool size of 0.14 mm [10]. This paper presents simulation results; however, it lacks comprehensive experimental validation to corroborate its findings. Without such validation, the reliability of the outcomes remains uncertain. Additionally, the study does not fully address the temperature profiles, which is necessary to understand their effects on residual stresses.

The molten pool experiences high temperatures and rapid cooling rates due to the concentrated energy source and the relatively short contact time. In the direct metal deposition (DMD) process for Ti6Al4V alloy, the cooling rate can reach approximately $7 \times 10^4$ K/s [12,29]. AM titanium alloy fabricated by EBM was reported to have low residual stresses, with DMD having low porosity, and SLM high residual stress [12,32]. Still, they have the advantage of having lower residual stress, and the parts processed utilizing an electron beam can be used without any stress-relieving processes. DMD produces high deposition rates with a higher layer thickness than other AM processes.

It was observed that no previous article had reported on investigating the reduction in energy consumption, machined part qualification process, and optimization during the machining of Ti6Al4V parts produced by the AM process. Hence, this review article will focus on this critical gap. Table 1 below summarizes findings from various articles focusing on the machining process, AM techniques, and machining responses. From the table, many researchers focused on low-speed machining (40 to 100 m/min) and dry cooling strategy as the cutting environment due to advantages in cleanness; however, few reports were found on the DMD powder-based AM process. However, there are limited articles that reported on the DMD powder-based fusion process to manufacture Ti6Al4V alloy parts for machining operations.

**Table 1.** Summary of previous articles on machinability of AM Ti6Al4V alloy.

| Reference | Machining Process | Machining Parameters | AM Techniques | Cutting Environment | Machining Responses |
|---|---|---|---|---|---|
| [15] | Turning | V = 45, 90, 180 m/min<br>f = 0.05, 0.1, 0.2 mm/rev<br>d = 0.5 mm | SLM | Dry | Surface roughness and cutting forces |
| [17] | Milling | V = 40, 60, 80 m/min<br>f = 0.06, 0.1, 0.2 mm/tooth<br>d = 1.0, 2.0 mm | SLM | Dry and MQL | Cutting forces and residual stress |
| [33] | Turning | V = 50, 80, 110 m/min<br>f = 0.1 mm/rev<br>d = 1.0 mm | EBM | Dry and cryogenic cooling | Cutting force and temperature |
| [34] | Turning | V = 50, 80 m/min<br>f = 0.1, 0.2 mm/rev<br>d = 0.25 mm | EBM | Dry and cryogenic conditions | Tool wear |
| [35] | Turning | V = 50, 80 m/min<br>f = 0.1, 0.2 mm/rev<br>d = 1.0 mm | EBM | Dry and cryogenic | Tool wear and surface roughness |
| [19] | Micro-Milling | V = 23.6, 31.4, 39.3, 47.1, and 55.0 m/min<br>f = 30, 60, and 90 mm/rev<br>d = 0.075 mm (axial) | SLM | MQL | Tool wear and surface burning |
| [20] | Face Milling | V = 55 m/min<br>f = 0.08 mm/rev<br>d = 0.5 mm | SLM | Dry | Surface roughness and cutting forces |
| [21] | Turning | V = 80 m/min<br>f = 0.2 mm/rev<br>d = 0.5 mm | SLM | Cryogenic | Surface roughness |
| [18] | Milling | Spindle speed = 4000–10,000 rpm<br>V = 50.24–125.6 m/min<br>f = 0.01–0.08 mm/tooth<br>d = 0.1–0.8 mm (axial) | SLM | Dry | Surface roughness, wear rate, hardness, microstructure, and adhesion |
| [23] | High-speed milling | V = 150, 200, and 250 m/min<br>f = 0.05, 0.07, and 0.09 mm/tooth<br>d = 8.0 mm (radial) and 0.5 mm (axial) | DMLS | Dry | Cutting forces, chip morphology, surface quality, and tool wear |
| [24] | Turning | V = 80 m/min<br>f = 0.1 and 0.2 mm/rev<br>d = 0.25 mm | DMLS | Dry and cryogenic ($LN_2$) | Surface roughness |
| [27] | Turning | V = 50 and 110 m/min<br>f = 0.2 mm/rev<br>d = 1.0 mm | DMLS, EBM, and Wrought | Dry | Surface roughness |
| [25] | Drilling | Spindle speed = 500–1200 rpm<br>f = 0.06, 0.09, 0.12, and 0.15 mm/rev<br>d = 12 mm (h) | DMLS | Dry | Surface roughness and tool wear |
| [28] | Drilling | V = 500, 800, 1200, and 1500 rev/min<br>f = 0.06, 0.09, 0.12, 0.15 mm/rev | HTDMLS | Dry | Chip morphology, surface integrity |
| [26] | Side Milling | V = 40, 80, 120, and 180 m/min<br>f = 0.08 mm/tooth<br>d = 1.0 mm (radial) and 10 mm (axial) | DMLS | Dry and supercritical CO2-based MQL | Milling force, subsurface microstructure evolution, residual stress, and crystallographic texture |

**Table 1.** *Cont.*

| Reference | Machining Process | Machining Parameters | AM Techniques | Cutting Environment | Machining Responses |
|---|---|---|---|---|---|
| [36] | Drilling and milling | Milling parameters<br>V = 80 m/min<br>f = 0.06 mm/rev<br>d = 30 mm (axial) and 1.0 mm (radial)<br>Drilling parameters<br>V = 9.0 m/min<br>f = 0.09 mm/rev<br>hole depth = 12.5 mm | WAAM (GTAW) | Dry | Surface roughness, cutting forces, and tool wear |
| [6] | Up-milling, down-milling, and slot-milling | V = 50, and 60 m/min<br>f = 0.12 mm/rev<br>d = 0.4 mm (axial) | WAAM (PAL) | Dry | Surface roughness |
| [37] | LAM-Milling | F =100 mm/min<br>d = −0.3 mm<br>Spindle speed (N) = 6000 rpm<br>Preheating temp—600 °C | DED | Dry | Surface roughness |
| [30] | Turning | V = 70 m/min<br>d = 1.25 mm<br>f = 0.15 mm/rev | DMD | Dry | Surface roughness |
| [31] | Side Milling | N = 4000 rpm<br>d = 0.6 mm<br>f = 0.05–0.13 mm/tooth | DMD | Dry and cooling water | Tool flank wear, cutting forces, and subsurface deformation |

Table 2 presents mechanical properties of Ti6Al4V alloy parts manufactured by the DMD process and compared with the ASTM standard.

**Table 2.** Mechanical properties of titanium alloy parts manufactured by DMD as built and heat-treated [7].

| Process | Yield Strength (MPa) | Ultimate Tensile Strength (MPa) | Percentage Elongation (%) |
|---|---|---|---|
| ASTM Standard | 827 | 896 | 10 |
| As deposited | 1105 + 19 | 1165 + 22 | 4 + 1 |
| Air-cooled at 950 °C | 975 + 15 | 1053 + 18 | 7.5 + 1 |
| The furnace cooled at 950 °C | 959 + 12 | 1045 + 16 | 10.5 + 1 |
| Air-cooled at 1050 °C | 931 + 16 | 1002 + 19 | 6.5 + 1 |
| The furnace cooled at 1050 °C | 900 + 14 | 951 + 15 | 7.5 + 1 |

## 3. Machinability of AM Ti6Al4V Alloy

Machinability is assessed based on factors such as tool wear, tool life, chip formation, cutting forces, temperature fields, burr size, and surface quality. To enhance productivity, tungsten carbide (WC) inserts, whether coated or uncoated, are commonly used for machining titanium alloys. Wet cutting environments help control heat generation and accumulation at the tool–workpiece interface, while dry cutting results in a cleaner working environment. In wet cutting conditions, lower temperatures at the cutting tip lead to reduced cutting forces. Additionally, a significant challenge in machining Ti6Al4V alloy is its chemical reactivity with the tool material, which can result in rapid tool wear due to either dissolution of the tool material or chemical reactions with the chip [38]. Ti6Al4V alloy's machinability depends on cutting force, tool life, missing temperature, burr size, chip formation, and surface integrity [39,40]. The elasticity of a material contributes a significant portion to determining its machinability [41].

### 3.1. Titanium Alloy

Titanium alloy, also known as Ti64, is extensively used for structural and engine components in the aerospace industry and for onshore and offshore equipment owing to its excellent corrosion resistance, high strength, and low density. Ti6Al4V alloy is the most widely used alloy, accounting for over half of all titanium goods used worldwide. In the 1950s, Ti6Al4V alloy was first fabricated for structural uses in the aircraft industry [12]. In addition to its widespread use in the aerospace industry, titanium and its alloys are utilized in various other applications, including surgical implants, heat exchangers, bioengineering, valve bodies, marine hardware, missile fuel tanks, compressors, and lightweight springs [42].

Titanium alloys can be classified into three classes based on their crystal structure, as follows [7,18,41,43]:

- Pure titanium, such as commercially pure Ti, has excellent corrosion resistance but low mechanical strength properties and good weldability. The addition of small amounts of Fe and O could increase its strength.
- Alpha and near-alpha class (α-phase), such as Ti3Al2.5V, contain alpha stabilizers and possess excellent creep resistance.
- Alpha-beta class (α–β-phase), such as Ti6Al4V and Ti5Al2.5Fe; this class at room temperature presents both 'alpha' and 'beta' phases. It is mainly used for mechanical applications requiring high strength and low density at raised temperatures.
- Beta class (β-phase), such as Ti5Al5Mo5V3Cr, contains a significant amount of beta stabilizers and is characterized by high density and hardenability. Moreover, β-phase has been known for its excellent biomedical properties and is used as an orthopedic (bone) implant.

At room temperature, titanium alloy exists as a stable closed packed hexagonal (HCP) structure called the alpha phase; it changes to a stable body-centered cubic (BCC) structure called the beta phase at higher temperatures (880 °C). The α-phase of titanium has an HCP structure with 12 primary slip systems. The α-phase exhibits higher strength, hardness, and toughness than the β-phase, which contains many β-phase additions and is a BCC structure containing standard 48 slip systems. Vanadium, niobium, and tantalum are β-phase stabilizers, while aluminum and tin are α-phase stabilizers [16,44–46]. The cited papers overlook important aspects, such as the focus on emerging technologies like AM, which are increasingly significant for titanium-based materials. Additionally, they do not address the cost and sustainability of titanium materials, factors that are critical for assessing their economic feasibility and industrial adoption.

Aluminum, vanadium, oxygen, hydrogen, zirconium, and palladium are the alloying elements of titanium. Aluminum and vanadium are the principal alloying elements. Aluminum offers corrosion resistance and strengthens solid solutions, while vanadium is a beta stabilizer that widens the temperature range to retain the beta properties. The corrosion resistance of the one-way scanning method was found to be superior to that of cross scanning. However, both methods demonstrated slightly lower corrosion resistance compared to wrought materials. This difference is likely due to variations in phase and element distribution, grain size, and crystal texture [47]. Table 3 shows the mechanical properties of different materials, with Ti6Al4V alloy having low density coupled with high strength and good corrosion resistance. Reports indicate that the Ti6Al4V alloy exhibits a corrosion rate of 5 μm per year, which is considered negligible compared to that of aluminum, of 30 μm per year [48,49].

**Table 3.** Mechanical properties of Ti6Al4V and other alloys [3,44].

| Property | Material | | | | | | |
|---|---|---|---|---|---|---|---|
| | **Ti** | **Ti10Vfe3Al (β-alloy)** | **Ti6Al4V2Sn (α-βalloy)** | **Ti6Al4V (α-β-alloy)** | **Ti8V6Cr4 Mo4Zr3Al (β-alloy)** | **Inconel 718** | **Al** |
| Density (g/cm$^3$) | 4.5 | 4.65 | 4.54 | 4.42 | 4.81 | 8.22 | 2.7 |
| Hardness (HRC) | 10–12 | 32 | 38 | 30–36 | 37–43 | 38–44 | 60 |
| Ultimate tensile strength (MPa) | 220 | 970 | 1050 | 950 | 1250 | 1350 | 310 |
| Yield strength (MPa) | 140 | 990 | 980 | 880 | 1150 | 1170 | 300 |
| Modulus of elasticity (GPa) | 116 | 110 | 110 | 113.8 | 102 | 200 | 68.3 |
| Ductility (%) | 54 | 9 | 14 | 14 | 15 | 16 | 17 |
| Fracture toughness. (MPa m$^{1/2}$) | 70 | - | 60 | 75 | 65 | 96.4 | 29 |
| Thermal conductivity (W/Mk) | 17 | 7.8 | 6.6 | 6.7 | 8.4 | 11.4 | 167 |
| Max. operating temperature (°C) | 150 | 315 | 315 | 315 | 315 | 650 | 170 |

In machining operations involving challenging materials such as Ti6Al4V alloy, substantial mechanical and thermal loads are generated, which may be detrimental to the performance and life of a cutting tool during the chip formation process [50]. The poor machinability of Ti6Al4V alloy is due to its outstanding mechanical properties, which are characterized by high energy consumption, low tool life, and inferior surface finishing [3]. A low thermal conductivity value results in heat accumulation at the tooltip, thus resulting in early tool failure. The lower value of thermal conductivity (5.5 to 25.0 W/mK, at temperatures ranging from 273 to 1073 K) of Ti6Al4V results in heat accumulation at the tooltip, thus resulting in early tool failure [40]. Table 4 represents the chemical properties of Ti6Al4V alloy reported by some researchers.

**Table 4.** Chemical composition of titanium alloy [3,6].

| Element | Al | V | Fe | Cu | Cr | Ti |
|---|---|---|---|---|---|---|
| Composition (Wt. %) | 5.7 | 4.2 | 0.15 | 0.003 | 0.0023 | 89.44 |

Turning is the most commonly used machining process for shaping titanium alloy parts. Key factors influencing the machinability of titanium alloys during turning include cutting parameters, tool geometry, and the cutting environment, particularly the use of cutting fluid. Cutting fluid serves to cool, lubricate, and facilitate chip removal during the machining of metallic materials. Given that manufacturing is energy-intensive, ongoing efforts are focused on developing new techniques to reduce energy consumption, especially in machining processes.

### *3.2. Material of a Cutting Tool*

The integrity of a cutting tool is primarily evaluated based on its ability to resist wear, particularly flank wear, which has a significant impact on tool edges and the dimensional accuracy of the workpiece. Tool materials can be classified according to their performance and durability. One commonly used coating material is titanium nitride (TiN), known for its excellent coating properties, which allow for increased cutting speeds and extended tool life; and coating material include titanium carbon nitride (TiCN), titanium aluminum nitride (TiAlN), and aluminum oxide ($Al_2O$) [51]. The purpose of the coating is to protect the tool from being worn. The report shows that coated inserts yield good results at higher cutting speed, feed rate and a depth of cut 4 μm thick [52] was chosen for the coating process with TiAlN during the cutting operation for titanium alloy parts [53]. This paper narrows its investigation to cutting speed, without exploring other critical parameters such as feed rate and depth of cut, both of which significantly impact surface integrity and

cutting force. Furthermore, it lacks attention to the lifecycle impact of titanium materials, an essential consideration for understanding their long-term performance and sustainability.

The tungsten or cemented carbide WC+Co tools contain tungsten, carbon, and cobalt. They have 6% content of the Co element. These are the most used cutting tools in machining processes and include straight-grade tungsten carbide and cobalt grade. Carbide tools possess excellent wear resistance and toughness properties even at high cutting temperatures above 600 °C and a maximum cutting speed of 300 m/min. Delicate grain structures were reported to have performed better against grains with larger sizes or with high cobalt content (10% Co). Also, TiCN-coated tools performed significantly better than CrN-coated tools in turning titanium alloy [38]. The following describe the properties and characteristics of different cutting tools:

- Carbon tool steel (0.6% to 1.5% C) having a maximum cutting speed of 5 m/min.
- Satellites are tungsten, molybdenum, or molybdenum–cobalt base grades with a maximum cutting speed of 100 m/min.
- High-speed steel (HSS) ratio 18:4:1 of W:Cr:V is the most applicable tool and possesses excellent toughness but low hardness among all types of cutting tools, with a maximum cutting speed of 33 m/min.
- Ceramic tools contain aluminum oxide ($Ai_2O_3$), $Cr_2O_3$, $Zr_2O$, TiN, or silicon nitride. They are referred to as having less toughness compared to carbide tools. The maximum cutting speed is 650 m/min.
- Special-purpose tools (up to 4500 HV) such as cubic boron nitride and polycrystalline cubic boron nitride with a maximum cutting speed of 800 m/min, a polycrystalline diamond with a top cutting speed of 1300 m/min. These are the less applicable cutting tools in the machining industry because of their high tool cost, low toughness, and high hardness compared to other cutting tools, showing that ceramic and carbide tools perform better at high cutting temperatures.

Several reports indicate that straight tungsten carbide (WC/Co) tools have demonstrated superior performance in nearly all machining processes involving titanium alloys. These tools offer enhanced wear resistance and durability, making them well-suited for the challenges associated with machining titanium [42,51,54]. It was indicated that these WC/Co alloys with a Co concentration of 6 Wt% and a minimum WC grain size of between 0.8 and 1.4 µm might achieve the best performance [54]. The carbide tool with H13A grade type K20 was found to perform excellently in the titanium alloy turning operation [3,53]. The cutting material must have the following properties when machining difficult-to-cut material (like titanium alloy):

- Excellent chipping resistance
- Hot hardness, necessary to maintain the high cutting temperature
- Good compressive strength
- Fatigue resistance and high toughness value, to withstand the cyclic machining forces generated
- Low chemical affinity with the titanium atom
- Outstanding thermal conductivity, to dissipate the heat generated quickly.

The limited machinability of titanium alloys is primarily due to their high reactivity with most cutting tool materials. Performing cutting operations in an inert environment has shown to enhance tool life by reducing chemical interactions between the tool and the material, even in conventional machining settings. However, during the machining of titanium alloys, the high-temperature accumulation between the tip of the workpiece, cutting tool, and chip results in tool coating failure and delamination [39]. The heat partition during machining titanium alloys was observed to be 80% transferred to the cutting tool, while only 20% was transferred to the chips [52]. Therefore, it might cause frequent loss or change of cutting tools, which leads to high machining costs. Due to the high machining costs in traditional processes, titanium alloys have drawn the utmost interest in metal additive manufacturing, reducing the cost in return [55]. Table 5 highlights the mechanical

properties of a tungsten carbide tool with high density and excellent thermal conductivity compared to Ti6Al4V alloy.

**Table 5.** Mechanical properties of a tungsten carbide tool [56].

| Property | Value |
|---|---|
| Density (kg/m$^3$) | $14.5 \times 10^3$ |
| Ultimate tensile strength (MPa) | 3000 |
| Young's modulus of elasticity (GPa) | 650 |
| Thermal conductivity (W/Mk) | 58.98 |
| Poisson ratio | 0.25 |
| Heat capacity (J/kg K) | 15.0018 |

### *3.3. Tool Geometry*

The cutting tool geometry refers to its dimensional design, which includes the rake angle, flank or clearance angle, and nose radius or cutting-edge radius. It was observed that the normal rake angle and normal flank angle of the cutting tool for WC CNMA432 were 15° and 6°, respectively, selected to perform an orthogonal cutting on titanium alloy, with the tool's cutting-edge radius of 0.030 mm, a 90° cutting edge angle, and a 0° cutting edge inclination angle. The author used no cutting fluid [56]. It was deduced that the cutting material workpiece suffering from compression would deform plastically [53].

Machining AM-based Ti6Al4V parts typically requires specialized cutting tools due to the material's high strength and toughness. Improper selection of cutting parameters can lead to accelerated tool wear, increasing energy consumption during machining. Reducing energy consumption is a complex challenge that requires optimizing cutting parameters, utilizing advanced tool materials and coatings, adopting sustainable cutting environments, and incorporating advanced technologies. Combining these strategies can produce more energy-efficient machining processes with economic and environmental benefits. Upgrading to more energy-efficient machining equipment, such as CNC machines or high-speed machining centers, can significantly reduce energy consumption. These machines were designed to operate with minimal waste, which not only saves energy but also reduces emissions associated with the manufacturing of the equipment itself. Several studies [3,15,19,20,34,36,57] have explored various machining techniques, including milling, turning, drilling, and grinding, to improve surface roughness and tool wear, reduce energy consumption, and reduce mechanical damage caused by drilling operations.

### *3.4. Selection of Cutting Conditions*

The selection of cutting conditions, environments, and inserts plays a crucial role in the effective machining of titanium alloys. Polycrystalline diamond (PCD) inserts have been reported to be particularly effective in high-speed machining processes, offering enhanced performance and tool life due to their superior hardness and wear resistance at elevated cutting speeds up to 150 m/min, Titanium diboride ($TiB_2$) is used for intermediate rates up to 100 m/min, and cubic boron nitride (CBN) tools for lower cutting speeds ideally for finishing cuts [40]. Cutting conditions played a vital role in the analysis of energy consumption and surface quality in the machining of titanium alloy [58].

The levels and cutting conditions, such as cutting speed, feed rate, and depth of cut, can be selected based on any previously reported work in the literature or tool manufacturers' guidelines, as listed in Table 6. Experiments can be repeated two or three times for data repeatability. However, a new insert needs to be used in each experimental run.

**Table 6.** Guidelines from manufacturers for turning heat-treated titanium alloy [59,60].

| Cutting Condition | Carbide Tool | Cast Alloy Tool | HSS Tool |
|---|---|---|---|
| Cutting speed (SFPM) | 75–275 | 75–275 | 30–50 |
| Feed rate (IPR) | 0.003–0.01 | 0.002–0.005 | 0.002–0.005 |
| Depth of cut (In) | 0.0003–0.03 | 0.003–0.03 | 0.0003–0.03 |

Hardness refers to a material's resistance to plastic deformation, often resulting from rapid cooling. It is typically measured using scales such as Vickers, Rockwell, or Brinell, with the hardness value indicating the material's (or cutting tool's) ability to resist deformation and achieve the desired surface finish. Studies have shown that hardness is a key factor in determining cutting forces and burr formation during micromachining processes [7]. A comparison of hardness and toughness across different cutting tools reveals that polycrystalline diamond (PCD) exhibits high hardness but low toughness. In contrast, high-speed steel (HSS) tools demonstrate low hardness combined with high toughness. Ceramics and coated carbide tools offer a balance, displaying moderate levels of both hardness and toughness, making them suitable for a range of machining applications [51].

### *3.5. Tool Wear Rate*

Tool wear is a gradual breakdown or failure of a cutting tool due to regular machining operation, and it can be identified as edge chipping, built-up edge, fracture, flank wear, etc. Tool life can be enhanced by the appropriate selection of cutting speed, feed rates, and cutting environment. Tool wear can be monitored by vibration signal measurement during the machining process. Tool material is expected to possess high hardness at elevated temperatures to withstand the stresses involved, chipping resistance, toughness, and fatigue resistance to resist the chip segmentation process, and good thermal conductivity to minimize thermal shock on the cutting tool. Another report showed that mixed ceramic silicon shows the highest wear rate of 2304 µm/min [43]. This paper primarily focuses on a specific cooling strategy utilizing liquid nitrogen, without exploring alternative cooling methods such as air cooling, oil-based cooling, or hybrid cooling techniques. This limited scope may restrict the applicability of the findings to broader machining contexts and does not provide a comprehensive understanding of the various cooling options available.

During high-speed machining of titanium alloys, the presence of compressive solid loads and elevated temperatures near the cutting edge significantly influences tool wear. Consequently, plastic deformation emerges as a critical factor in the wear analysis of various tool materials [54]. Turning titanium alloy at 51 m/min with TiCN or CrN-coated inserts developed high flank wear in the flank edges, as shown in Figure 4, in addition to notch wear [52]. One of the disadvantages of uncoated tools is that they reach their maximum process temperature easily compared to coated tools. A common sign that a tool's life has ended is flank wear [61]. The advantage of employing cutting fluids was found to increase the tool life [24].

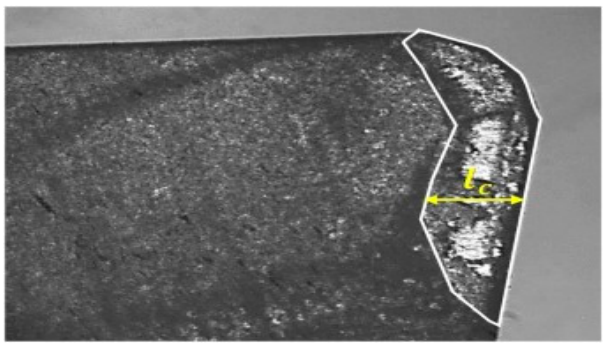


**Figure 4.** SEM image of a tool insert's wear, with a contact length of $l_c$ [3].

An H13 uncoated carbide insert was employed in turning titanium parts and optimizing four responses: SCE, Ra, R, and MRR [62]. Straight carbide insert (WC/Co) cutting tools were reported to be superior when machining titanium alloys, irrespective of the wear mechanism [63]. Straight-grade WC is the best tool material for cutting tool life [64]. The report shows that coated carbide offers no significant advantage due to its increased wear rates [42,65].

### *3.6. Chip Morphology*

High cutting speeds lead to more frequent chip segments, especially in turning titanium alloy [3]. Scanning electron microscopy (SEM) is an optical investigation methodology that produces high-resolution visual images such as those of chip morphology. The chip morphology helps to analyze the cutting forces and the energy consumption during machining by calculating the chip compression ratio, which can be obtained by dividing uncut chip thickness $(t_1)$ by cut (deformed) chip thickness $(t_2)$ and chip shear angle $(\phi)$, as shown in Figure 5. Different methods used by some researchers [3,66,67] for describing the chip morphology were reported, where the researcher considered a minimum chip thickness and maximum chip thickness to calculate the degree of segmentation $(G)$, as shown in the equation below. The results show that chip formation depends on cutting speed and uncut chip thickness.

$$G = \frac{t_{2max} - t_{2min}}{t_{2max}} \quad (1)$$

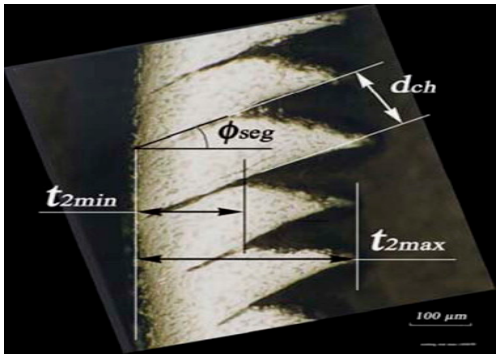


**Figure 5.** Segmented chip and parameters according to the maximum and minimum chip thickness [67].

Another interesting report described the chip morphology using an undeformed chip cross-sectional area of the line $(A, B)$ and its characteristic length of $(L)$, as shown in Figure 6. The results show that the slipping angle $(\theta)$ of the segmented chip was 55°, higher than that of a continuous chip, at 38°. The characteristic length was observed to be increased with feed rate, but independent of cutting velocity [66].

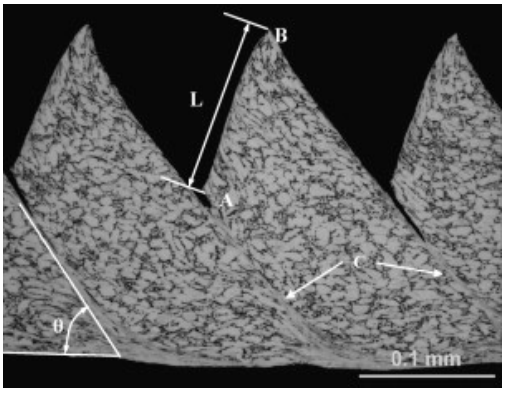


**Figure 6.** Chip morphology according to the slipping angle and characteristic length [66].

The chip compression ratio ($r$) was found to be an essential factor in estimating energy consumption efficiency, cutting forces, chip formation, and shear angle during machining [3]. The larger value of r results in a smaller shear plane angle and leads to larger strain and energy consumption, as shown in Figure 7.

$$r = \frac{h_1}{h_2} \tag{2}$$

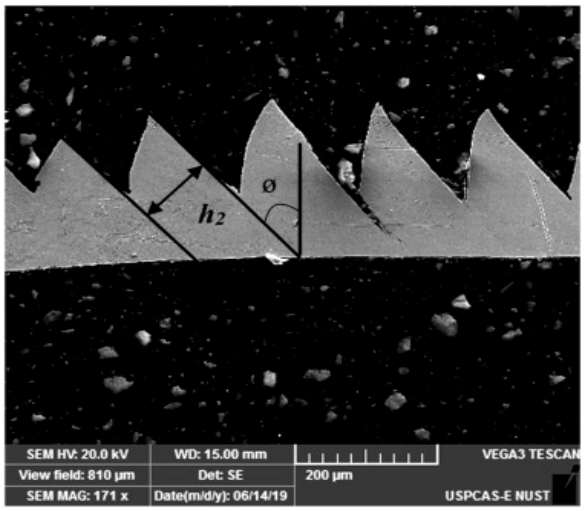


**Figure 7.** SEM image of chip formation in turning titanium alloy [3].

### *3.7. Machining Forces Generated*

The cutting forces generated during the machining operation are normal force ($F_n$), tangential force ($F_t$), cutting force ($F_c$), and feed rate force ($F_a$). The coating layer minimizes friction at the tool–chip interface, reducing the cutting forces and heat produced by friction. Additionally, the coating layer serves as a shield protecting against thermal shocks in milling [51]. Cutting stresses (energies) can be measured using a force dynamometer and a load cell to measure forces, or by monitoring power usage [68].

The cutting force $(F_C)$ and tangential force $(F_t)$ can be determined from Equations (3) and (4), respectively. Frictional $(F)$ and resultant force $(R)$ can be obtained from Equations (5) and (6), respectively. SCE can be determined from either Equation (7) or (8), and shear plane angle $(\phi)$ can be determined from Equation (9), while chip compression ratio $(r)$ can be determined from Equation (10) [53,69–72].

$$F_C = R\cos(\lambda - \alpha) \tag{3}$$

$$F_t = R\sin(\lambda - \alpha) \tag{4}$$

$$F = R\sin\lambda \tag{5}$$

$$R = \frac{F_S}{\cos\theta} \tag{6}$$

$$SCE = \frac{P_{cut}}{MRR} \tag{7}$$

$$SCE = \frac{F_C}{w \cdot t_0} \tag{8}$$

$$tan\phi = \frac{rcos\alpha}{1 - sin\alpha} \tag{9}$$

$$r = \frac{t_1}{t_2} \tag{10}$$

The observed weak cutting forces can be attributed to the low friction resulting from the high rake angle of 20 degrees selected for the machining process [53]. In the machining of titanium alloys, the high heat level at the cutting tip may sometimes approach 1100 °C. Due to this high temperature, the cutting edge may deteriorate rapidly and become dull due to the elevated temperature close to the cutting zone [51]. It was observed that at any cutting speed selected and if the cutting temperature was less than the beta transit of titanium alloy (880 °C), no phase transition occurred during orthogonal cutting of titanium alloy [53]. The different types of heat generated because of tool-to-workpiece interaction and the deformation zones have been reported [51].

It was reported that energy stored during a cutting operation generates more softening effects in titanium alloy [53]. Another apparent reason for the heat accumulation in the titanium workpiece is that the workpiece is diffused with oxygen and nitrogen from the air, which hardens the surface layer when the cutting zone temperature surpasses 600–700 °C [51]. This report lacks a comparative analysis of different cutting tools and materials specifically in the context of machining titanium alloys. Such an analysis would be instrumental in understanding the advantages and disadvantages of various tools under identical conditions, thereby providing valuable insights for optimizing machining processes. It was reported that short contact time between the tool and workpiece due to high cutting velocities affected heat transfer efficiency; in other words, low cutting speed improves heat transfer effectively [68]. Another study showed that an increase in cutting speed results in lower cutting forces that lead to low SCE due to the thermal softening effects during machining [73].

### *3.8. Surface Roughness*

The surface roughness (Ra) measurement refers to the average texture of a finished machined surface, and it plays an important part in the functionality and reliability of a final product. It is a predominant requirement for the machined part to perform satisfactorily and depends on cutting conditions, workpiece, and tool material properties. The surface roughness can be measured using different means, such as contact-based devices and digital holographic microscopes.

High surface roughness can be desirable in certain applications; however, it is often undesirable, particularly when surface contact necessitates low friction for mating with another surface or when a smooth appearance is required to minimize wear on materials [74]. It was concluded that a cutting speed of 70 m/min and a depth of cut of 0.1 mm was insignificant in increasing the surface roughness, whereas a feed rate of 0.1 mm/rev contributed to an increase of 83.69% in surface roughness [75]. Surface roughness of less than 2 µm can be achieved by selecting a suitable combination of a considerable depth of cut and high spindle speed [46]. It was reported that maximum surface roughness of 2.16 µm and tool flank wear of 0.201 mm could be achieved with a cutting speed of 250 m/min, feed rate of 0.1 mm/rev, and depth of cut of 0.1 mm [76]. Another report shows that surface roughness decreased with increased nose radius. Therefore, the roughness value of a machined surface was reduced by 27.90% and 26.70% for the predicted and measured values, respectively [77,78]. Cutting forces and tool wear variations for a machined part were insignificant in affecting roughness values of both wrought and smelted laser-manufactured Ti6Al4V parts, even below 2 µm [7,79]. The surface roughness value increases with an increased cutting speed of up to 80 m/min and decreases with further cutting speed increases [80].

It was observed that the surface finish can be improved by increasing the cutting speed. However, the built-up edge formation on the tooltip subsequently deteriorates the workpiece quality due to high surface roughness at low cutting speed. The quality of a surface finish decreases as the feed rate increases because of the high friction developed due to a large amount of chips flowing on the cutting tool edge.

### 3.9. Energy Consumption

The estimated power can be divided into air cut ($P_I$) and actual or total cut ($P_T$) powers. It was reported that energy and power consumption could be investigated using a quality analyzer (CA8331) manufactured by Chauvin Arnoux (Asnières-sur-Seine, France) to measure and control the energy consumed during the machining process [81]. The mathematical difference between $P_A$ and $P_T$ will determine the cutting power ($P_C$) needed for material removal during the cycle, as shown in Equation (12) [62]. Power cut represents the energy consumed by machine tools to achieve a workpiece's final surface finish [82].

Modern manufacturing requires reducing the electrical energy consumption of machine tool operations to achieve cleaner and more efficient production [82,83]. Manufacturing equipment widely used in the industry includes machine tools, which share a significant part of the energy consumed [84,85]. As the machining process progresses, the primary reason for tool wear is seen in the variation of the specific cutting energy. Tool life is also affected by increased cutting speed and the feed rate [62]. It was reported that the up-milling machining process consumes more energy than the down-milling process, which is 8.5% on average [86]. Nguyen employed multi-response optimization to investigate energy consumption during dry milling. The results indicate that a reduction in cutting forces also leads to a decrease in SCE [77]. However, this paper neglects to address tool wear and tool life, and it fails to incorporate other cooling strategies, such as oil-based cooling or hybrid cooling. This oversight may overlook significant variables that influence machining efficiency and surface integrity.

Accurately selecting cutting parameters reduces energy consumption to an optimum level with high surface quality [87,88]. SCE and MRR were observed to be reduced by 16% and 127%, respectively, at a higher cutting speed of 125 m/min [3]. As the cutting condition increases, the energy efficiency is reported to increase during milling operation. As such, most of the energy was consumed by the supporting system [86]. The power of machine tool feature transitions was reduced by 28.60% [83]. According to some reports, the world economy depends mainly on energy savings because the sector that consumes energy is the manufacturing industry [2,89,90]. Cryogenic machining has been reported to have reduced the energy consumption of a machine tool by 80% at a cutting speed of 200 m/min [91]. It was reported that tool life increased by 28.9% and 38.6% in the dry cutting environment and deep cryogenically treated WC tools, respectively [40]. The main reasons for the energy consumption during machining processes is resistance to the cutting forces and movement of the spindle, as well as adjusting the speed up or down. To determine the required energy consumed during the cutting process or chip removal, it is vital to consider the different power dissipated during air cutting ($P_I$), cutting process ($P_C$), and total energy ($P_T$) from Equation (11):

$$P_{Total} = \sqrt{3} V I Cos\sigma \tag{11}$$

where $V$ is the CNC vertical operating voltage in ($V$)

$I$ = the current indicated by the ammeter in ($A$)

$Cos\sigma$ is the phase angle.

Equation (12) determines the cutting power during chip removal by subtracting the idle power from the actual power dissipated [92].

$$P_{Cutting} = P_{Total} - P_{Iddle} \tag{12}$$

$P_{Cutting}$ is an essential factor affecting cutting force, tool wear, surface roughness, and chip formation [89].

$$SEC\left(\frac{J}{mm^3}\right) = \frac{P_{Total}}{MRR}\left(\frac{KW}{\frac{mm^3}{s}}\right) \tag{13}$$

Energy map development in machining refers to the graphical representation of energy consumption into low, medium, and high levels to identify the safe zone in the machining process. Several studies [3,93] have used this mapping approach to develop

energy maps during machining. Energy mapping involves plotting feed rate (rev/mm) against cutting speed (m/min) to divide the map into three energy zones: low, medium, and high. One report shows that SCE of <1.00 is classified as a low energy zone, 1.00 to 1.10 as a medium energy zone, and >1.10 as a high energy zone [3]. This study primarily focused on varying cutting speed and feed rates without considering tool geometry or depth of cut, which can significantly influence tool wear and energy consumption. While the research successfully identifies zones of wear and energy consumption, it lacks a comprehensive analysis of the underlying mechanisms driving these phenomena, thereby limiting the depth of understanding of tool wear processes. Additionally, the energy consumption maps developed may not account for variations in machine tool dynamics and environmental factors, which could potentially impact their applicability in diverse manufacturing settings. The report shows that in the milling process of Ti6Al4V alloy, SCE, the depth of cut, and cutting speed increase with a decrease in the feed rate [94]. Another researcher showed that energy consumption was heavily dependent on the cutting speed and feed rate. However, an increase in both leads to lower energy consumption in turning of Ti6Al4V alloy [73]. The report shows that an increase in feed rate leads to an increase in the shear plane angle and results in lowering the SCE by 27% per 1 kg of the MRR, as indicated in the energy map [93].

### *3.10. Optimization Process*

The cutting speed, feed rate, and depth of cut are the key cutting parameters that must be optimized in machining experiments to enhance the quality and efficiency of machined parts. Proper optimization of these parameters significantly impacts surface finish, dimensional accuracy, and overall process efficiency, making them critical for achieving high-quality results in machining operations [95]. The report shows that the optimization process reduced surface roughness and specific cutting energy by 2% and 6%, whereas it increased the material removal rate and tool life by 34% and 7%, respectively [92].

Dr. Genichi Taguchi first developed the Taguchi method, which is employed in engineering analysis to determine the optimum combinations of process conditions for improving performance characteristics in manufacturing systems [89]. The Taguchi method was combined with statistical analysis to optimize the machining process for design purposes [88]. It was widely acknowledged that the Taguchi approach is a solid and efficient technique for reducing energy intensity, significantly increasing process performance with minimal testing, production, and cycle time to determine the optimal conditions for the objectives [78,96–98].

Grey relational analysis is another optimization technique that converts multiple response values into a single grey relational grade value. It can be applied in decision-making to find the most significant relations in the complicated context system characterized by multiple impute [96]. The main advantage of grey relational analysis is that it simplifies the optimization process by converting the numerous performance characteristics problem into a single performance characteristic [82]. The report shows that during the machining of Ti6Al7Nb alloy, the feed rate was the most influencing factor; about 11.3% enhancement was achieved compared to the previous value by using the GRA optimization process [96]. In addition, multi-objective optimization can achieve the sustainable goal of machining Ti6Al4V alloys with a high material removal rate, longer tool life, and minimum energy consumption. A multi-objective analysis is an optimization process that involves establishing multiple objectives by combining multiple prediction models to obtain an objective model's final and optimal solution for the evaluation indices [99]. In implementing energy-saving efficiently, a multi-objective analysis has been conducted between cutting conditions and energy consumption to optimize energy efficiency and meet other manufacturing requirements [90].

Analysis of variance (ANOVA) is a statistical analysis package that assesses the significant involvement of cutting parameters on output responses. This is achieved by computing the sequential sum of squares for the given parameters at a stated confidence level. ANOVA

was performed to assess the most significant cutting conditions for material removal rate, tool wear, and surface roughness in machining operations with the determination of the optimal parameters [96,100,101].

MINITAB 21® is statistical software that designs the experiment for the optimization process, where the software investigates the significance levels of the cutting conditions (v, f, and d) on the machining responses. It was reported that the interaction effect (vxv, fxv) was more significant than the individual effect in investigating the effect of cutting conditions on the machining responses using statistical software, where ANOVA was achieved at a 95% confidence level. Table 7 represents many studies that have optimized the machining process using the Taguchi method, Grey relational analysis, ANN, and regression. However, the Taguchi method was found to be the most effective.

**Table 7.** Summary of literature on optimization in the machining of Ti6Al4V alloy.

| Reference | Optimization Method | Cutting Environment | Cutting Condition | Machining Responses |
|---|---|---|---|---|
| [96] | Grey Taguchi | Wet and dry | V = 60, 80, and 100 m/min<br>f = 0.08, 0.16, and 0.24 mm/rev<br>d = 0.2, 0.3, and 0.4 mm | Surface roughness, tool wear, power consumption, and material removal rate. |
| [102] | Grey relational analysis based on Taguchi | MQL | V = 50, 80, and 100 m/min<br>f = 1 mm/rev<br>d = 1.5 mm | Surface roughness and flank wear. |
| [96] | Grey-Taguchi approach | Dry | V = 35, 70, and 105 m/min<br>f = 0.08, 0.12 and 0.16 mm/rev<br>d = 0.1, 0.2 and 0.3 mm | Tool wear and surface roughness. |
| [92] | Grey relational analysis, Taguchi | Dry | V = 50, 100, and 150 m/min<br>f = 0.12, 0.16 and 0.20 mm/rev<br>d = 1, 1.5 and 2 mm | Tool wear rate, SCE, surface roughness, material removal rate |
| [103] | Grey relational analysis, ANN, and regression | Dry | V = 140, 224, and 315 m/min<br>f = 0.051, 0.071 and 0.102 mm/rev<br>d = 0.5, 0.75 and 1 mm | Cutting force temperature and surface roughness |
| [57] | Taguchi | Dry | Drilling speed (V) = 20, and 165 mm/min | Induced mechanical damage by drilling operation |
| [96] | Grey relational analysis | Dry | V = 174, 420, and 930 m/min<br>f = 0.08, 0.28 and 0.52 mm/rev<br>d = 0.4, 0.6 and 0.8 mm | Material removal rate, tool flank wear, tool nose wear, and surface roughness. |
| [68] | Taguchi $L_{27}$ ($3^{13}$) | Dry | V = 250, 500, 750, 1000, 1250, 1500, 1750, and 2000 m/min<br>f = 0.1, 0.2, 0.3, and 0.4 mm/rev<br>d = 4.1 mm | Chip formation and cutting forces |

### *3.11. Qualification of Machined Parts for Assembly*

The AM parts can be machined to precise specifications, making them suitable for prototype applications, one-time parts, and mass production of stock components. The precision and consistency achieved in the machining of these parts enhance the reliability of the final product, which is especially crucial in critical onshore, offshore, medical and transportation applications. As industries often require replacement parts, the demand for machined components continues to grow. Geometrical product specification (GPS) provides guidelines for the qualification processes of profile and surface texture dimensions, ensuring the accuracy of surface roughness measurements [101]. Whenever any part in machinery or equipment suffers wear and tear, or breaks, it can be replaced with a perfectly fitted machined component, hence extending equipment life. Standards and specifications, such as ISO 9001 [104], AS9100, and ISO 13485 [105], set the foundation for defining qualification

requirements. It was noticed that a limited number of standards and specifications are present in the AM-process parts for assembly [106].

The qualification process employs both non-destructive and destructive testing methods to verify that components meet the specified quality standards for their intended applications. These methods are crucial for ensuring the safety, reliability, and overall quality of machined parts. The process typically begins with a visual inspection of the machined component, during which the dimensional accuracy is assessed for compliance with ISO designation standards. ISO 13485 was established to qualify the AM Ti6Al4V alloy for medical implants accepted for applying heart valve frames [107]. EN ISO 3452 and ASTME 1417 present guidelines for detecting a crack on the threads and surface AM hydraulic manifold by dye penetrant [108]. ISO 21920-2:2021 [109] is a proper qualification process that helps in ensuring that machined parts are of the required standards in terms of quality. It includes dimensional accuracy, surface finish, material integrity, and many other vital specifications. A researcher can produce goods that have quality by keeping up with all these standards, hence reducing defects and variability in products.

### *3.12. Finite Element Analysis*

The Johnson–Cook (J–C) model is the best model for predicting material behavior that involves dynamic loading with enormous strain hardening, high strain rates, and elevated temperature. The J–C model is one of the constitutive equations employed to simulate the thermo-elastoplastic behavior of the work piece's Ti6Al4V alloy and the WC-Co tool material [56]. This model has the advantage of predicting material behavior at different strain rates and temperatures but with the disadvantage of requiring extensive experimental data [110]. The J–C model, the most popular model used to predict high strain rate deformations, was employed for the workpiece material. The J–C plasticity model contains analytical strengthening rate and temperature dependence models [68].

Several mathematical models created based on the material's plastic deformation principles can express cutting force, temperatures, stress, or strain [7]. The first part of the J–C model is the strain hardening effect, the second part has the strain rate effect or (viscous effect), and the last is the thermal softening effect. The J–C model material parameters (A, B, C, m, and n) are determined by the split Hopkinson pressure bar (SHPB) mechanical test conducted at strain rates from about 800 to 3300 $s^{-1}$ and temperatures from 20 to 1100 °C [111]. SHPB has some imperfections that might compromise the test result validity, including the swinging effects that flow stress shows, especially at low strain values, because the flow stress always depends heavily on the strain pathway [112]. Due to this limitation, some researchers were able to modify the J–C model equation to predict the flow stress in machining operations accurately. For example, the J–C model equation was modified to consider the strain-softening effect to predict the flow stress [113], and the temperature effect was considered in the modified J–C model. The result was acceptable and validated using the modified J–C models [111].

It was observed that no previous model has been reported for predicting the cutting forces and flow stress during the turning operation for cylindrical bars of Ti6Al4V alloy used in the AM (DMD) process. Therefore, this reviewed article focuses on this critical gap. Table 8 below summarizes the findings of different models from various themes, focusing on the investigated parameters, material type, and model type. The J–C material model is the most used plastic model due to its ability to incorporate strain hardening, strain rates, and thermal softening effects.

**Table 8.** Synopsis of the application of different models from the literature.

| Model | Formula | Coefficients | Investigated Parameters | Type of Material | Reference |
|---|---|---|---|---|---|
| Johnson–Cook | $\sigma = (A + B\varepsilon^n)\left(1 + C\ln\frac{\dot{\varepsilon}}{\dot{\varepsilon}_0}\right)\left[1 - \left(\frac{T - T_0}{T_{melt} - T_0}\right)^m\right]$ | A, B, C, m, n | Flow stress | Wrought Ti6Al4V alloy | [114,115] |
| Johnson–Cook | $\sigma = (A + B\varepsilon^n)\left(1 + C\ln\frac{\dot{\varepsilon}}{\dot{\varepsilon}_0}\right)\left[1 - \left(\frac{T - T_0}{T_{melt} - T_0}\right)^m\right]$ | A, B, C, m, n | Cutting forces and chip morphology | Al 6061-T6 | [68] |
| Johnson–Cook | $\sigma = (A + B\varepsilon^n)\left(1 + C\ln\frac{\dot{\varepsilon}}{\dot{\varepsilon}_0}\right)\left[1 - \left(\frac{T - T_0}{T_{melt} - T_0}\right)^m\right]$ | A, B, C, m, n | Cutting temperature and tool wear | Wrought Ti6Al4V alloy | [56] |
| Johnson–Cook | $\sigma = (A + B\varepsilon^n)\left(1 + C\ln\frac{\dot{\varepsilon}}{\dot{\varepsilon}_0}\right)\left[1 - \left(\frac{T - T_0}{T_{melt} - T_0}\right)^m\right]$ | A, B, C, m, n | Chip morphology and adiabatic shear banding | Refractory Ti6Al4V alloy | [110,111] |
| Johnson–Cook | $\sigma = (A + B\varepsilon^n)\left(1 + C\ln\frac{\dot{\varepsilon}}{\dot{\varepsilon}_0}\right)\left[1 - \left(\frac{T - T_0}{T_{melt} - T_0}\right)^m\right]$ | A, B, C, m, n | Strain ($\varepsilon$), strain rate ($\dot{\varepsilon}$), and temperature | Brass | [112] |
| Power Law (PL) | $\sigma = \sigma_0\varepsilon^n\left(\frac{\dot{\varepsilon}}{\dot{\varepsilon}_0}\right)^m\left(\frac{T}{T_0}\right)^{-v}$ | $\sigma_0$, m, n, U | | | |
| Oxley Strain History | $\overline{\sigma} = \sigma_0\left(T, \dot{\varepsilon}\right) * \varepsilon^{n(T,\dot{\varepsilon})}$<br>$\overline{\sigma} = \sigma_0\left(T, \dot{\varepsilon}\right)\left(\int_{straini\ pass}^{'} e^{\left(\frac{k}{n}\right)T}(\dot{\varepsilon})^{\frac{-m}{n}} d\varepsilon\right)^n$<br>$\overline{\sigma} = \sigma_0\overline{\varepsilon}^n\left(\frac{\dot{\overline{\varepsilon}}}{\dot{\varepsilon}_0}\right)^m \exp\frac{G}{T}$ | $\sigma_0\left(T, \dot{\overline{\varepsilon}}\right)$, $n\left(T, \dot{\overline{\varepsilon}}\right)$<br>$\sigma_0\left(T, \dot{\varepsilon}\right)$, $k, m, n$ | Cutting forces, cutting temperature, and flow stress | AlSl 1045 | [113] |
| Vinh Zerilli-Armstrong (ZA) | For BCC structure<br>$\overline{\sigma} = C_0 + C_1\exp\left(-C_3T + C_4T\ln\frac{\dot{\overline{\varepsilon}}}{\dot{\varepsilon}_0}\right) + C_5\varepsilon^n$<br>For FCC structure<br>$\sigma = C_0 + C_2\varepsilon^{\frac{1}{2}}exp\left[\left(-C_3T + C_4\ln\left(\frac{\dot{\overline{\varepsilon}}}{\dot{\varepsilon}_0}\right)\right)T\right]$ | $\sigma_0$, m, n, G<br>$\sigma_0$, $C_0$, $C_2$, $C_3$, $C_4$, $C_5$ | Dislocation mechanics | Inconel 718 | [114] |

It was found that the J–C model shows a poor prediction of cutting forces at higher cutting speeds, up to 2000 m/min in orthogonal cutting of Al 6061-T6 [68]. However, regarding the Ti6Al4V alloy, reports indicate that the J–C model has several limitations. These include inaccuracies in capturing phase transformations and strain hardening saturation, as well as neglecting the effects of fracture or damage accumulation and microstructural variations within the Ti6Al4V alloy [116,117]. Future research directions aimed at addressing these limitations may involve the development of a numerical model that modifies the J–C model to better predict microstructural effects, including grain size, phase changes, and texture formation. Additionally, it would be beneficial to incorporate more comprehensive damage criteria, such as micro-crack nucleation, into the modified J–C model. One report showed that the J–C model was able to predict the milling forces when the preheating temperature exceeded 300 °C, and the milling forces were found to be reduced significantly in the milling operation of Ti6Al4V alloy, which was due to the thermal softening effect of the workpiece [31]. The J–C model shows a high plastic strain value on the chip contact side with the tool [115]. The modified Arrhenius model was more accurate in predicting flow stress than the Zerilli–Armstrong and Rusinek–Klepaczko models [107]. Some reports indicated the degradation in the mechanical behavior of a composite material that was caused by the initiation of damage using FEA, and the results were affected significantly by the depth of cut and fiber orientation rather than the tool edge and rake angle [118]. The J–C model shows that chip morphology depends considerably on the adiabatic shear zones, which rely intensely on cutting parameters such as cutting forces and temperature [110]. Another researcher used optimized J–C model parameters to calculate the flow stress under different conditions; the calculated results showed excellent agreement with the experimental results reported, with less than 4% error [108]. Tables 9 and 10 provide the required material constants and mechanical and physical properties for numerical analysis using the J–C model. The crack initiates at the free surface of the chip and propagates toward the tool, developing into micro-cracks during the machining operation as reported [119]. J–C model captures the essential characteristics required to simulate cutting forces, chip morphology, and flow stress accurately. It emerges from this model that while accounting for material thermal softening is necessary, it is not sufficient that the model should also incorporate strain-softening to represent a material's behaviours as reported by many researchers [112,120–123].

**Table 9.** Mechanical properties of Ti6Al4V alloy for J–C model [56].

| Property | Value |
|---|---|
| Density (kg/m$^3$) | $4.43 \times 10^3$ |
| Ultimate tensile strength (MPa) | 950 |
| Tensile yield strength (MPa) | 880 |
| Young's modulus of elasticity (GPa) | 113.8 |
| Thermal conductivity (W/Mk) | 17 |
| Poisson ratio | 0.32 |
| Heat capacity (J/kg K) | 526 |

**Table 10.** Material constants of J–C model parameters for the tool and workpiece [56].

| Constant | A | B | C | m | n | $T_O$ (°C) | $T_{Melting}$ (°C) |
|---|---|---|---|---|---|---|---|
| Ti6Al4V | 782.7 | 498.4 | 0.028 | 1 | 0.28 | 20 | 1668 |
| WC/Co | 0.003 | 8.0471 | 0.000 | 0.179 | 0.0003 | 20 | 1372 |

## 4. Summary of AM and Conventionally Manufactured Titanium Alloy

The AM Ti6Al4V parts need post-processing due to inconsistency in surface hardness, residual stresses, and roughness, which is carried out by machining. Although the post-processing of AM titanium is still very efficient compared to conventionally processing parts (casting, molding, forging, etc.), it should be noted that since titanium machining is also challenging, it needs to be thoroughly investigated and optimized for minimum energy consumption. Even though the machining of conventional titanium alloy has been extensively studied, the machining of AM titanium is significantly different, with the cutting forces observed to be about 55–70% higher compared to those for conventional titanium parts [6,74]. Higher cutting forces lead to increased energy consumption during the machining of Ti6Al4V parts produced through additive manufacturing (AM). The machinability of these parts presents unique challenges, including high hardness and strength, as well as residual stresses. These factors contribute to elevated energy consumption, a higher tool wear rate, and increased surface roughness in the machining process.

## 5. Conclusions

This paper has presented a systematic review of the machinability of AM Ti6A4V alloy, covering the wide range of AM techniques used to manufacture titanium parts. The effects of cutting conditions, stresses generated during AM processes on the energy consumption during machining of Ti6Al4V parts produced from AM techniques, FEA models for machining processes, and the qualification process were examined critically. The following key points were noted, which will aid in the machinability of AM Ti6Al4V alloy.

- It can be concluded that the machinability of a Ti6Al4V alloy is very challenging due to its low thermal conductivity. The AM titanium alloy was more difficult due to its resulting higher residual stresses, which could lead to high cutting forces in addition to the low thermal conductivity of the Ti6Al4V alloy.
- It was also deduced that energy maps plotted (feed rate against cutting speed) can be used to identify and classify energy consumption into low, medium, and high.
- The DMD-based process is the least reported and used among the AM techniques. Hence, this article finds a gap for recommendation as part of the methodology approach.
- It was reported that a laser scanning speed of 1200 mm/s at a more prominent spot size yields a low porosity during AM processing of titanium alloy.
- It was shown that the Johnson–Cook model was the model most predominantly employed in the numerical analysis of the machining process due to its ability to predict both the lower and higher cutting forces and stresses and its smaller number of constants.

- It was observed that the Johnson–Cook model was unable to predict the cutting forces at higher cutting speeds of up to 2000 m/min for Al 6061-T6 alloy.
- Multi-objective optimization can achieve the sustainable goal of machining Ti6Al4V alloys with a high material removal rate, longer tool life, and minimum energy consumption. The Taguchi method was found to be more effective than other optimization methods.
- There were limited or no articles to review regarding the qualification of machined parts for assembly manufactured by the AM process. Therefore, this research finds another exciting gap to fill.
- The focus will be developing a numerical model that represents the modified J–C model as a way to incorporate the prediction of microstructural changes such as grain size, phase changes, and texture formation. To develop a modified J–C model in a way to incorporates enlarged damage criteria, such as micro-crack nucleation, is important.
- Finite element modeling can be further integrated with experimental results to enhance the understanding of machining performance in AM-produced Ti6Al4V alloy parts.
- The energy consumption maps may be further developed to investigate the variations in machine tool dynamics and environmental factors, which could potentially impact their applicability in diverse manufacturing settings.

**Funding:** The APC was funded by the Author Voucher discount code (2157477d2db34e3e).

**Acknowledgments:** The author appreciates receiving the PhD studentship funding from Robert Gordon University, Aberdeen, Scotland, UK, to support this research.

**Conflicts of Interest:** The author declares no conflicts of interest.

## List of Notations

| Symbol | Definition | Unit |
|---|---|---|
| $A$ | J–C model initial yield strength | MPa |
| $B$ | J–C model strength coefficient | MPa |
| $C$ | J–C model strain rate constant | - |
| $n$ | J–C model strain hardening exponent | - |
| $m$ | J–C model thermal softening | - |
| $f$ | Frictional force | - |
| $F_c$ | Cutting force along cutting speed direction | N |
| $\theta$ | Angle between resultant force and line AB | o |
| $\phi$ | The shear angle between the shear plane | o |
| $\alpha$ | Rake angle | o |
| $\sigma$ | Flow stress | MPa |
| $\varepsilon$ | Equivalent strain | - |
| $l\dot{\varepsilon}$ | Equivalent strain rate | $s^{-1}$ |
| $t_1$ | Uncut chip thickness | mm |
| $t_2$ | Cut chip thickness | mm |
| $v$ | Cutting speed | m/min |
| $f$ | Feed rate | mm/rev |
| $d$ | Depth of cut | mm |
| $MRR$ | Material removal rate | $mm^3$/min |
| $R$ | Wear rate | $mm^3$/N |
| $Ra$ | Surface roughness | um |
| $SCE$ | Specific cutting energy | J/$mm^3$ |
| $RPM$ | Revolutions per minute | N |
| $P_a$ | Actual power cut | W |
| $P_{air}$ | Air power cut | W |
| $CNC$ | Computer numerical control | - |
| $GMAW$ | Gas metal arc welding | - |

| | | |
|---|---|---|
| *GTAW* | Gas tungsten arc welding | - |
| *PAL* | Plasma arc welding | - |
| *DMD* | Direct metal deposition | - |
| *DED* | Directed energy deposition | - |
| *DMLS* | Direct metal laser sintering | - |
| *EBM* | Electron beam melting | - |
| *WAAM* | Wire + arc additive manufacturing | - |
| *FEA* | Finite element analysis | - |
| *AM* | Additive manufacturing | - |
| *CAD* | Computer-aided design | - |
| *CAM* | Computer-aided manufacturing | - |

## References


1. Rosli, N.A.; Alkahari, M.R.; bin Abdollah, M.F.; Maidin, S.; Ramli, F.R.; Herawan, S.G. Review on effect of heat input for wire arc additive manufacturing process. *J. Mater. Res. Technol.* **2021**, *11*, 2127–2145. [CrossRef]
2. He, K.; Wang, L.; Li, X. Review of the energy consumption and production structure of China's steel industry: Current situation and future development. *Metals* **2020**, *10*, 302. [CrossRef]
3. MYounas, M.; Jaffery, S.H.I.; Khan, A.; Khan, M. Development and analysis of tool wear and energy consumption maps for turning of titanium alloy (Ti6Al4V). *J. Manuf. Process.* **2021**, *62*, 613–622. [CrossRef]
4. Younas, M.; Sambo, A.M.; Asim, T.; Saharudin, S. Assessment of Machinability of Ti6Al4V Alloy Under Dry Conditions. *MATEC Web Conf.* **2024**, *401*, 06005. [CrossRef]
5. Tofail, S.A.M.; Koumoulos, E.P.; Bandyopadhyay, A.; Bose, S.; O'Donoghue, L.; Charitidis, C. Additive manufacturing: Scientific and technological challenges, market uptake and opportunities. *Mater. Today* **2018**, *21*, 22–37. [CrossRef]
6. Veiga, F.; Gil Del Val, A.; Suárez, A.; Alonso, U. Analysis of the machining process of titanium Ti6Al-4V parts manufactured by wire arc additive manufacturing (WAAM). *Materials* **2020**, *13*, 766. [CrossRef]
7. Li, G.; Chandra, S.; Rashid, R.A.R.; Palanisamy, S.; Ding, S. Machinability of additively manufactured titanium alloys: A comprehensive review. *J. Manuf. Process.* **2022**, *75*, 72–99. [CrossRef]
8. Ramakrishnan, P. Welding Metallurgy. *Indian Weld. J.* **1972**, *4*, 89. [CrossRef]
9. Yang, Q.; Zhang, P.; Cheng, L.; Min, Z.; Chyu, M.; To, A.C. Finite element modeling and validation of thermomechanical behavior of Ti6Al4V in directed energy deposition additive manufacturing. *Addit. Manuf.* **2016**, *12*, 169–177. [CrossRef]
10. Parry, L.; Ashcroft, I.; Wildman, R. Understanding the effect of laser scan strategy on residual stress in selective laser melting through thermo-mechanical simulation. *Addit. Manuf.* **2016**, *12*, 1–15. [CrossRef]
11. Bontha, S.; Klingbeil, N.W. *Thermal Process Maps for Controlling Microstructure in Laser-Based Solid Freeform Fabrication*; The University of Texas at Austin: Austin, TX, USA, 2003.
12. Liu, S.; Shin, Y.C. Additive manufacturing of Ti6Al4V alloy: A review. *Mater. Des.* **2019**, *164*, 107552. [CrossRef]
13. Vastola, G.; Zhang, G.; Pei, Q.; Zhang, Y.-W. Controlling of residual stress in additive manufacturing of Ti6Al4V by finite element modeling. *Addit. Manuf.* **2016**, *12*, 231–239. [CrossRef]
14. Liu, Y.; Yang, Y.; Wang, D. A study on the residual stress during selective laser melting (SLM) of metallic powder. *Int. J. Adv. Manuf. Technol.* **2016**, *87*, 647–656. [CrossRef]
15. Polishetty, A.; Shunmugavel, M.; Goldberg, M.; Littlefair, G.; Singh, R.K. Cutting Force and Surface Finish Analysis of Machining Additive Manufactured Titanium Alloy Ti6Al4V. *Procedia Manuf.* **2017**, *7*, 284–289. [CrossRef]
16. Dutta, B.; Froes, F.H.S. The Additive Manufacturing (AM) of titanium alloys. *Met. Powder Rep.* **2017**, *72*, 96–106. [CrossRef]
17. Ming, W.; Chen, J.; An, Q.; Chen, M. Dynamic mechanical properties and machinability characteristics of selective laser melted and forged Ti6Al4V. *J. Mater. Process. Technol.* **2019**, *271*, 284–292. [CrossRef]
18. Su, Y.; Li, L.; Wang, G. Machinability performance and mechanism in milling of additive manufactured Ti6Al4V with polycrystalline diamond tool. *J. Manuf. Process.* **2022**, *75*, 1153–1161. [CrossRef]
19. Khaliq, W.; Zhang, C.; Jamil, M.; Khan, A.M. Tool wear, surface quality, and residual stresses analysis of micro-machined additive manufactured Ti–6Al–4V under dry and MQL conditions. *Tribol. Int.* **2020**, *151*, 106408. [CrossRef]
20. Milton, S.; Morandeau, A.; Chalon, F.; Leroy, R. Influence of Finish Machining on the Surface Integrity of Ti6Al4V Produced by Selective Laser Melting. *Procedia CIRP* **2016**, *45*, 127–130. [CrossRef]
21. Lizzul, L.; Bertolini, R.; Ghiotti, A.; Bruschi, S. Effect of AM-induced Anisotropy on the Surface Integrity of Laser Powder Bed Fused Ti6Al4V Machined Parts. *Procedia Manuf.* **2020**, *47*, 505–510. [CrossRef]
22. Alsaddah, M.; Khan, A.; Groom, K.; Mumtaz, K. Diode area melting of Ti6Al4V using 808 nm laser sources and variable multi-beam profiles. *Mater. Des.* **2022**, *215*, 110518. [CrossRef]
23. Zhang, H.; Dang, J.; Ming, W.; Xu, X.; Chen, M.; An, Q. Cutting responses of additive manufactured Ti6Al4V with solid ceramic tool under dry high-speed milling processes. *Ceram. Int.* **2020**, *46*, 14536–14547. [CrossRef]
24. Sartori, S.; Bordin, A.; Ghiotti, A.; Bruschi, S. Analysis of the Surface Integrity in Cryogenic Turning of Ti6Al4 v Produced by Direct Melting Laser Sintering. *Procedia CIRP* **2016**, *45*, 123–126. [CrossRef]

25. Dang, J.; Liu, G.; Chen, Y.; An, Q.; Ming, W.; Chen, M. Experimental investigation on machinability of DMLS Ti6Al4V under dry drilling process. *Mater. Manuf. Process.* **2019**, *34*, 749–758. [CrossRef]
26. Cai, C.; An, Q.; Ming, W.; Chen, M. Microstructure- and cooling/lubrication environment-dependent machining responses in side milling of direct metal laser-sintered and rolled Ti6Al4V alloys. *J. Mater. Process. Technol.* **2022**, *300*, 117418. [CrossRef]
27. Rotella, G.; Imbrogno, S.; Candamano, S.; Umbrello, D. Surface integrity of machined additively manufactured Ti alloys. *J. Mater. Process. Technol.* **2018**, *259*, 180–185. [CrossRef]
28. Ming, W.; Dang, J.; An, Q.; Chen, M. Chip formation and hole quality in dry drilling additive manufactured Ti6Al4V. *Mater. Manuf. Process.* **2020**, *35*, 43–51. [CrossRef]
29. Kasperovich, G.; Hausmann, J. Improvement of fatigue resistance and ductility of TiAl6V4 processed by selective laser melting. *J. Mater. Process. Technol.* **2015**, *220*, 202–214. [CrossRef]
30. Oyelola, O.; Crawforth, P.; M'Saoubi, R.; Clare, A.T. Machining of Additively Manufactured Parts: Implications for Surface Integrity. *Procedia CIRP* **2016**, *45*, 119–122. [CrossRef]
31. Li, S.; Zhang, B.; Bai, Q. Effect of temperature buildup on milling forces in additive/subtractive hybrid manufacturing of Ti6Al4V. *Int. J. Adv. Manuf. Technol.* **2020**, *107*, 4191–4200. [CrossRef]
32. Zhai, Y.; Galarraga, H.; Lados, D.A. Microstructure, static properties, and fatigue crack growth mechanisms in Ti6Al4V fabricated by additive manufacturing: LENS and EBM. *Eng. Fail. Anal.* **2016**, *69*, 3–14. [CrossRef]
33. Umbrello, D.; Bordin, A.; Imbrogno, S.; Bruschi, S. 3D finite element modelling of surface modification in dry and cryogenic machining of EBM Ti6Al4V alloy. *CIRP J. Manuf. Sci. Technol.* **2017**, *18*, 92–100. [CrossRef]
34. Bordin, A.; Bruschi, S.; Ghiotti, A.; Bariani, P. Analysis of tool wear in cryogenic machining of additive manufactured Ti6Al4V alloy. *Wear* **2015**, *328–329*, 89–99. [CrossRef]
35. Bruschi, S.; Bertolini, R.; Bordin, A.; Medea, F.; Ghiotti, A. Influence of the machining parameters and cooling strategies on the wear behavior of wrought and additive manufactured Ti6Al4V for biomedical applications. *Tribol. Int.* **2016**, *102*, 133–142. [CrossRef]
36. Hoye, N.; Cuiuri, D.; Rashid, R.A.R.; Palanisamy, S. Machining of gtaw additively manufactured Ti6Al4V structures. *Int. J. Adv. Manuf. Technol.* **2018**, *99*, 313–326. [CrossRef]
37. Woo, W.-S.; Kim, E.-J.; Jeong, H.-I.; Lee, C.-M. Laser-Assisted Machining of Ti6Al4V Fabricated by DED Additive Manufacturing. *Int. J. Precis. Eng. Manuf. Green Technol.* **2020**, *7*, 559–572. [CrossRef]
38. Younas, M.; Khan, M.; Jaffery, S.H.I.; Khan, Z.; Khan, N. Investigation of tool wear and energy consumption in machining Ti6Al4V alloy with uncoated tools. *Int. J. Adv. Manuf. Technol.* **2024**, *132*, 3785–3799. [CrossRef]
39. Maranchik, J., Jr.; Snider, R.E. *Machining of Titanium Alloys*; Springer: Berlin/Heidelberg, Germany, 1968.
40. Saini, A.; Pabla, B.; Dhami, S. Developments in cutting tool technology in improving machinability of Ti6Al4V alloy: A review. *Proc. Inst. Mech. Eng. Part B J. Eng. Manuf.* **2016**, *230*, 1977–1989. [CrossRef]
41. Rashid, R.A.R.; Sun, S.; Wang, G.; Dargusch, M.S. Machinability of a near beta titanium alloy. *Proc. Inst. Mech. Eng. Part B J. Eng. Manuf.* **2011**, *225*, 2151–2162. [CrossRef]
42. AMachado, A.R.; Wallbank, J. Machining of Titanium and its Alloys—A Review. *Proc. Inst. Mech. Eng. Part B J. Eng. Manuf.* **1990**, *204*, 53–60. [CrossRef]
43. von Turkovich, B.F.; Durham, D.R. *Machining of Titanium and Its Alloys*; The Metallurgical Society of AIME: San Ramon, CA, USA, 1982; pp. 257–274.
44. Avila, J.D.; Bose, S.; Bandyopadhyay, A. *Additive Manufacturing of Titanium and Titanium Alloys for Biomedical Applications*; Elsevier Inc.: Amsterdam, The Netherlands, 2018. [CrossRef]
45. ASaurabh, A.; Meghana, C.M.; Singh, P.K.; Verma, P.C. Titanium-based materials: Synthesis, properties, and applications. *Mater. Today Proc.* **2022**, *56*, 412–419. [CrossRef]
46. Lou, Y.; Wu, H. Effect of parameters on surface roughness during the ultra-precision polishing of titanium alloy. *PLoS ONE* **2022**, *17*, e0272387. [CrossRef]
47. Zhou, X.; Xu, D.; Geng, S.; Fan, Y.; Liu, M.; Wang, Q.; Wang, F. Mechanical properties, corrosion behavior and cytotoxicity of Ti6Al4V alloy fabricated by laser metal deposition. *Mater. Charact.* **2021**, *179*, 111302. [CrossRef]
48. Almanza, E.; Pérez, M.; Rodríguez, N.; Murr, L. Corrosion resistance of Ti6Al4V and ASTM F75 alloys processed by electron beam melting. *J. Mater. Res. Technol.* **2017**, *6*, 251–257. [CrossRef]
49. Titakis, C.; Vassiliou, P. Evaluation of 4-Year Atmospheric Corrosion of Carbon Steel, Aluminum, Copper and Zinc in a Coastal Military Airport in Greece. *Corros. Mater. Degrad.* **2020**, *1*, 159–186. [CrossRef]
50. Soori, M.; Arezoo, B. Cutting tool wear minimization in drilling operations of titanium alloy Ti6Al4V. *Proc. Inst. Mech. Eng. Part J J. Eng. Tribol.* **2023**, *237*, 1250–1263. [CrossRef]
51. Hosseini, A.; Kishawy, H.A. *Cutting Tool Materials and Tool Wear*; Springer: Berlin/Heidelberg, Germany, 2014; pp. 31–56. [CrossRef]
52. Jaffery, S.H.; Khan, M.; A Sheikh, N.; Mativenga, P. Wear mechanism analysis in milling of Ti6Al4V alloy. *Proc. Inst. Mech. Eng. Part B J. Eng. Manuf.* **2013**, *227*, 1148–1156. [CrossRef]
53. Hassan, A.; Khan, M.A.; Younas, M.; Jaffery, S.H.I.; Khan, M.; Ahmed, N.; Awang, M. Impact of dry and cryogenic cutting medium on shear angle and chip morphology in high-speed machining of titanium alloy (Ti6Al4V). *Int. J. Automot. Mech. Eng.* **2024**, *21*, 11316–11331. [CrossRef]

54. Ezugwu, E.O.; Wang, Z.M. Materials Processing Technology Titanium alloys and their machinability a review. *J. Mater. Process. Technol.* **1997**, *68*, 262–274. [CrossRef]
55. Zhang, T.; Liu, C.-T. Design of titanium alloys by additive manufacturing: A critical review. *Adv. Powder Mater.* **2022**, *1*, 100014. [CrossRef]
56. Shao, F.; Liu, Z.; Wan, Y.; Shi, Z. Finite element simulation of machining of Ti6Al4V alloy with thermodynamical constitutive equation. *Int. J. Adv. Manuf. Technol.* **2010**, *49*, 431–439. [CrossRef]
57. Starost, K.; Njuguna, J. A review on the effect of mechanical drilling on polymer nanocomposites. *IOP Conf. Series: Mater. Sci. Eng.* **2014**, *64*, 012031. [CrossRef]
58. Akkuş, H.; Yaka, H. Experimental and statistical investigation of the effect of cutting parameters on surface roughness, vibration and energy consumption in machining of titanium 6Al-4V ELI (grade 5) alloy. *Measurement* **2021**, *167*, 108465. [CrossRef]
59. Uddeholm Elmax, ®. *Cutting Data Recommendations*; Uddeholm: Hagfors Municipality, Sweden, 2007.
60. Guidelines for Selecting Cutting Parameters Titanium. Available online: https://www.bing.com/ck/a?!&&p=7f666767268a904c57dd7a7530b8c01530471dc42837dc2a36c2b43c17b115b6JmltdHM9MTczMDg1MTIwMA&ptn=3&ver=2&hsh=4&fclid=21f10f52-962f-61b7-0676-1a7497876054&psq=61.+Guidelines+for+selecting+cutting+parameters+Titanium.&u=a1aHR0cHM6Ly93d3cua2VubmFtZXRhbC5jb20vY29udGVudC9kYW0va2VubmFtZXRhbC9rZW5uYW1ldGFsL2NvbW1vbi9SZXNvdXJjZXMvQ2F0YWxvZ3MtTGl0ZXJhdHVyZS9NZXRhbHdvcmtpbmcvVGl0YW5pdW1fbWF0ZXJpYWxfbWFjaGluaW5nX2d1aWRlX0Flcm9zcGFjZS5wZGY&ntb=1 (accessed on 4 November 2024).
61. Hourmand, M.; Sarhan, A.A.D.; Sayuti, M.; Hamdi, M. A Comprehensive Review on Machining of Titanium Alloys. *Arab. J. Sci. Eng.* **2021**, *46*, 7087–7123. [CrossRef]
62. Younas, M.; Jaffery, S.H.I.; Khan, M.; Ahmad, R.; Ali, L.; Khan, Z.; Khan, A. Tool Wear Progression and its Effect on Energy Consumption in Turning of Titanium Alloy (Ti6Al4V). *Mech. Sci.* **2019**, *10*, 373–382. [CrossRef]
63. Dearnley, P.; Grearson, A. Evaluation of principal wear mechanisms of cemented carbides and ceramics used for machining titanium alloy IMI 318. *Mater. Sci. Technol.* **2012**, *2*, 47–58. [CrossRef]
64. Hughes, J.I.; Sharman, A.R.C.; Ridgway, K. The effect of cutting tool material and edge geometry on tool life and workpiece surface integrity. *Proc. Inst. Mech. Eng. Part B J. Eng. Manuf.* **2006**, *220*, 93–107. [CrossRef]
65. Hartung, P.; Kramer, B.; von Turkovich, B. Tool Wear in Titanium Machining. *CIRP Ann.* **1982**, *31*, 75–80. [CrossRef]
66. Sun, S.; Brandt, M.; Dargusch, M. Characteristics of cutting forces and chip formation in machining of titanium alloys. *Int. J. Mach. Tools Manuf.* **2009**, *49*, 561–568. [CrossRef]
67. Sutter, G.; List, G. Very high speed cutting of Ti6Al4V titanium alloy—Change in morphology and mechanism of chip formation. *Int. J. Mach. Tools Manuf.* **2013**, *66*, 37–43. [CrossRef]
68. Akram, S.; Jaffery, S.H.I.; Khan, M.; Fahad, M.; Mubashar, A.; Ali, L. Numerical and experimental investigation of Johnson–Cook material models for aluminum (AL 6061-t6) alloy using orthogonal machining approach. *Adv. Mech. Eng.* **2018**, *10*, 1–14. [CrossRef]
69. Naik, P.; Naik, A. Determination of Flow Stress Constants by Oxley's Theory. Available online: www.ijltemas.in (accessed on 4 November 2024).
70. Laakso, S.V.A.; Niemi, E. Determination of material model parameters from orthogonal cutting experiments. *Proc. Inst. Mech. Eng. Part B J. Eng. Manuf.* **2016**, *230*, 848–857. [CrossRef]
71. Milton, M.C.; Shaw, C. *Metal Cutting Principles*; Oxford University Press: Oxford, UK, 2005.
72. Sambo, A.M.; Younas, M.; Njuguna, J. Effects of cutting conditions on the cutting forces in machining additively manufactured Ti6Al4V alloy. *MATEC Web Conf.* **2024**, *401*, 06003. [CrossRef]
73. Pervaiz, S.; Deiab, I.; Mihai Nicolescu, C. Energy Consumption and Surface Finish Analysis of Machining Ti6Al4V. Available online: https://www.researchgate.net/publication/266731984 (accessed on 4 November 2024).
74. Escamilla-Salazar, I.G.; Torres-Treviño, L.M.; González-Ortíz, B.; Zambrano, P.C. Machining optimization using swarm intelligence in titanium (6Al 4V) alloy. *Int. J. Adv. Manuf. Technol.* **2013**, *67*, 535–544. [CrossRef]
75. Km, R.; Sahoo, A.K.; Routara, B.C.; Panda, A.; Kumar, R. Study on machinability characteristics of novel additive manufactured titanium alloy (Ti6Al4V) fabricated by direct metal laser sintering. *Proc. Inst. Mech. Eng. Part C J. Mech. Eng. Sci.* **2023**, *237*, 865–885. [CrossRef]
76. Mathonsi, T.N.; Laubscher, R.F.; Gupta, K. On Machinability of Titanium Grade 4 under Minimum Quantity Lubrication Assisted High Speed Machining. *IOP Conf. Series: Mater. Sci. Eng.* **2018**, *430*, 012013. [CrossRef]
77. Nguyen, T.-T. Prediction and optimization of machining energy, surface roughness, and production rate in SKD61 milling. *Measurement* **2019**, *136*, 525–544. [CrossRef]
78. Soori, M.; Arezoo, B. Minimization of surface roughness and residual stress in abrasive water jet cutting of titanium alloy Ti6Al4V. *Proc. Inst. Mech. Eng. Part E J. Process. Mech. Eng.* **2023**, *238*, 1613–1625. [CrossRef]
79. Li, G.; Rashid, R.A.R.; Ding, S.; Sun, S.; Palanisamy, S. Machinability Analysis of Finish-Turning Operations for Ti6Al4V Tubes Fabricated by Selective Laser Melting. *Metals* **2022**, *12*, 806. [CrossRef]
80. Woodruff, G.W.; Liang, S.Y.; Garmestani, H.; Kurfess, T.; Shih, D.S.; Saldana, C. *Predictive Modeling for Material Microstructure Affected Machining*; Georgia Institute of Technology: Atlanta, GA, USA, 2018.
81. Cozzolino, E.; Franchitti, S.; Borrelli, R.; Pirozzi, C.; Astarita, A. Energy consumption assessment in manufacturing Ti6Al4V electron beam melted parts post-processed by machining. *Int. J. Adv. Manuf. Technol.* **2023**, *125*, 1289–1303. [CrossRef]

82. Hanafi, I.; Khamlichi, A.; Cabrera, F.M.; Almansa, E.; Jabbouri, A. Optimization of cutting conditions for sustainable machining of PEEK-CF30 using TiN tools. *J. Clean. Prod.* **2012**, *33*, 1–9. [CrossRef]
83. Hu, L.; Liu, Y.; Peng, C.; Tang, W.; Tang, R.; Tiwari, A. Minimising the energy consumption of tool change and tool path of machining by sequencing the features. *Energy* **2018**, *147*, 390–402. [CrossRef]
84. Cao, H.; Li, H.; Cheng, H.; Luo, Y.; Yin, R.; Chen, Y. A carbon efficiency approach for life-cycle carbon emission characteristics of machine tools. *J. Clean. Prod.* **2012**, *37*, 19–28. [CrossRef]
85. Gamage, J.R.; DeSilva, A.K.; Chantzis, D.; Antar, M. Sustainable machining: Process energy optimisation of wire electrodischarge machining of Inconel and titanium superalloys. *J. Clean. Prod.* **2017**, *164*, 642–651. [CrossRef]
86. Liu, Z.; Sealy, M.; Li, W.; Zhang, D.; Fang, X.; Guo, Y.; Liu, Z. Energy consumption characteristics in finish hard milling. *J. Manuf. Process.* **2018**, *35*, 500–507. [CrossRef]
87. Yurdakul, M. Effect of cutting parameters on consumed power in industrial granite cutting processes performed with the multi-disc block cutter. *Int. J. Rock Mech. Min. Sci.* **2015**, *76*, 104–111. [CrossRef]
88. Camposeco-Negrete, C. Optimization of cutting parameters for minimizing energy consumption in turning of AISI 6061 T6 using Taguchi methodology and ANOVA. *J. Clean. Prod.* **2013**, *53*, 195–203. [CrossRef]
89. Younas, M.; Khan, M.; Jaffery, S.H.I.; Ali, L.; Ahmad, R. Process Parameters and Its Effect on Surface Roughness during Turning Ti6Al4V Alloy. In *Advances in Manufacturing Technology XXXIII*; IOS Press: Amsterdam, The Netherlands, 2019; pp. 303–308.
90. Moreira, L.; Li, W.; Lu, X.; Fitzpatrick, M. Energy-Efficient machining process analysis and optimisation based on BS EN24T alloy steel as case studies. *Robot. Comput. Manuf.* **2019**, *58*, 1–12. [CrossRef]
91. Shokrani, A.; Dhokia, V.; Newman, S.T. Energy conscious cryogenic machining of Ti6Al4V titanium alloy. *Proc. Inst. Mech. Eng. Part B J. Eng. Manuf.* **2018**, *232*, 1690–1706. [CrossRef]
92. Younas, M.; Jaffery, S.H.I.; Khan, M.; Khan, M.A.; Ahmad, R.; Mubashar, A.; Ali, L. Multi-objective optimization for sustainable turning Ti6Al4V alloy using grey relational analysis (GRA) based on analytic hierarchy process (AHP). *Int. J. Adv. Manuf. Technol.* **2019**, *105*, 1175–1188. [CrossRef]
93. Warsi, S.S.; Jaffery, S.H.I.; Ahmad, R.; Khan, M.; Ali, L.; Agha, M.H.; Akram, S. Development of energy consumption map for orthogonal machining of Al 6061-T6 alloy. *Proc. Inst. Mech. Eng. Part B J. Eng. Manuf.* **2018**, *232*, 2510–2522. [CrossRef]
94. Tlhabadira, I.; Daniyan, I.; Masu, L.; Mpofu, K. Development of a model for the optimization of energy consumption during the milling operation of titanium alloy (Ti6Al4V). *Mater. Today: Proc.* **2021**, *38*, 614–620. [CrossRef]
95. Duong, T.-H.; Kim, H.-C.; Lee, D.-Y. Selection of machining conditions for microchannels in ultraprecision diamond turning. *Proc. Inst. Mech. Eng. Part B J. Eng. Manuf.* **2013**, *227*, 1558–1570. [CrossRef]
96. Khan, M.; Warsi, S.S.; Jaffery, S.H.I.; Ahmad, R.; Younas, M. Analysis of Energy Consumption in Orthogonal Machining of Al 6061-T6 Alloy. In *Advances in Manufacturing Technology XXXIII*; IOS Press: Amsterdam, The Netherlands, 2019; pp. 327–333.
97. Khan, M.A.; Jaffery, S.H.I.; Khan, M.; Younas, M.; Butt, S.I.; Ahmad, R.; Warsi, S.S. Multi-objective optimization of turning titanium-based alloy Ti6Al4V under dry, wet, and cryogenic conditions using gray relational analysis (GRA). *Int. J. Adv. Manuf. Technol.* **2020**, *106*, 3897–3911. [CrossRef]
98. Jaffery, S.H.I.; Younas, M.; Khan, M.; Ali, L. Energy consumption analysis in turning Ti6Al4V alloy. In Proceedings of the 2020 IEEE 11th International Conference on Mechanical and Intelligent Manufacturing Technologies (ICMIMT), Cape Town, South Africa, 20–22 January 2020; pp. 18–21.
99. Zhang, Y.; Ji, H. Wear optimization of titanium alloy cutter milled with microtextured ball-end milling cutter. *Adv. Mech. Eng.* **2014**, *12*, 1–14. [CrossRef]
100. Khan, M.A.; Jaffery, S.H.I.; Khan, M.; Younas, M.; Butt, S.I.; Ahmad, R.; Warsi, S. Statistical analysis of energy consumption, tool wear and surface roughness in machining of Titanium alloy (Ti6Al4V) under dry, wet and cryogenic conditions. *Mech. Sci.* **2019**, *10*, 561–573. [CrossRef]
101. Kumar, S.L. Experimental investigations and empirical modeling for optimization of surface roughness and machining time parameters in micro end milling using Genetic Algorithm. *Measurement* **2018**, *124*, 386–394. [CrossRef]
102. Gupta, A.; Kumar, R.; Kumar, H.; Garg, H. Optimization of process parameters during machining of Ti6Al7Nb by grey relational analysis based on Taguchi. *J. Physics: Conf. Ser.* **2019**, *1240*, 012121. [CrossRef]
103. Shah, D.R.; Bhavsar, S.N. An experimental investigation of tool nose radius and machining parameters on TI6AL4V (ELI) using grey relational analysis, regression and ANN models. *Int. J. Data Netw. Sci.* **2019**, *3*, 291–304. [CrossRef]
104. *ISO 9001*; Quality Management Systems. ISO: Geneva, Switzerland, 2015.
105. *ISO 13485*; Medical Devices. ISO: Geneva, Switzerland, 2016.
106. Seifi, M.; Gorelik, M.; Waller, J.; Hrabe, N.; Shamsaei, N.; Daniewicz, S.; Lewandowski, J.J. Progress Towards Metal Additive Manufacturing Standardization to Support Qualification and Certification. *JOM* **2017**, *69*, 439–455. [CrossRef]
107. du Preez, W.B. Towards Qualification of Additively Manufactured Ti6Al4V (ELI) Medical Implants. *JOM* **2019**, *71*, 655–661. [CrossRef]
108. Arena, M.; Ambrogiani, P.; Raiola, V.; Bocchetto, F.; Tirelli, T.; Castaldo, M. Design and Qualification of an Additively Manufactured Manifold for Aircraft Landing Gears Applications. *Aerospace* **2023**, *10*, 69. [CrossRef]
109. *ISO 21920-2:2021*; Geometrical Product Specifications (GPS)—Surface Texture: Profile. ISO: Geneva, Switzerland, 2021.
110. Rodean, C.; Beju, L.-D.; Rusu, G.; Popp, M. The Usage of the Johnson-Cook Constitutive Model in the Finite Element Analysis of the Caulking Process. *MATEC Web Conf.* **2019**, *290*, 03013. [CrossRef]

111. Sima, M.; Özel, T. Modified material constitutive models for serrated chip formation simulations and experimental validation in machining of titanium alloy Ti6Al4V. *Int. J. Mach. Tools Manuf.* **2010**, *50*, 943–960. [CrossRef]
112. Zhang, Y.; Outeiro, J.; Mabrouki, T. On the selection of Johnson-Cook constitutive model parameters for Ti6Al4V using three types of numerical models of orthogonal cutting. *Procedia CIRP* **2015**, *31*, 112–117. [CrossRef]
113. Calamaz, M.; Coupard, D.; Girot, F. A new material model for 2D numerical simulation of serrated chip formation when machining titanium alloy Ti6Al4V. *Int. J. Mach. Tools Manuf.* **2008**, *48*, 275–288. [CrossRef]
114. Kotkunde, N.; Krishnamurthy, H.N.; Puranik, P.; Gupta, A.K.; Singh, S.K. Microstructure study and constitutive modeling of Ti6Al4V alloy at elevated temperatures. *Mater. Des.* **2014**, *54*, 96–103. [CrossRef]
115. Chen, G.; Ren, C.; Yu, W.; Yang, X.; Zhang, L. Application of genetic algorithms for optimizing the Johnson–Cook constitutive model parameters when simulating the titanium alloy Ti6Al4V machining process. *Proc. Inst. Mech. Eng. Part B J. Eng. Manuf.* **2012**, *226*, 1287–1297. [CrossRef]
116. Yapan, Y.F.; Korkmaz, H.G.; Toros, S.; Türköz, M. Experimental and numerical investigation of the damage state of Ti6Al4V alloy sheet in the tensile test, hydraulic bulging, and hydroforming processes. *Int. J. Adv. Manuf. Technol.* **2024**, *132*, 4585–4605. [CrossRef]
117. Hou, X.; Liu, Z.; Wang, B.; Lv, W.; Liang, X.; Hua, Y. Stress-strain curves and modified material constitutive model for Ti6Al4V over thewide ranges of strain rate and temperature. *Materials* **2018**, *11*, 938. [CrossRef]
118. Calamaz, M.; Coupard, D.; Nouari, M.; Girot, F. Numerical analysis of chip formation and shear localisation processes in machining the Ti6Al4V titanium alloy. *Int. J. Adv. Manuf. Technol.* **2011**, *52*, 887–895. [CrossRef]
119. Ducobu, F.; Rivière-Lorphèvre, E.; Filippi, E. Numerical contribution to the comprehension of saw-toothed Ti6Al4V chip formation in orthogonal cutting. *Int. J. Mech. Sci.* **2014**, *81*, 77–87. [CrossRef]
120. Osorio-Pinzon, J.C.; Abolghasem, S.; Casas-Rodriguez, J.P. Predicting the Johnson Cook constitutive model constants using temperature rise distribution in plane strain machining. *Int. J. Adv. Manuf. Technol.* **2019**, *105*, 279–294. [CrossRef]
121. Adibi-Sedeh, A.H.; Vaziri, M.; Pednekar, V.; Madhavan, V.; Ivester, R. Investigation of the Effect of Using Different Material Models on Finite Element Simulations of Machining. In Proceedings of the 8th CIRP International Workshop on Modeling of Machining Operations, Chemnitz, Germany, 10–11 May 2005; pp. 215–224.
122. Gurusamy, M.M.; Rao, B.C. On the performance of modified Zerilli-Armstrong constitutive model in simulating the metal-cutting process. *J. Manuf. Process.* **2017**, *28*, 253–265. [CrossRef]
123. Zenia, S.; Ben Ayed, L.; Nouari, M.; Delamézière, A. Numerical analysis of the interaction between the cutting forces, induced cutting damage, and machining parameters of CFRP composites. *Int. J. Adv. Manuf. Technol.* **2015**, *78*, 465–480. [CrossRef]